arXiv:astro-ph/0102374v1 21 Feb 2001

Properties of Globular Cluster Systems in Nearby Early-type Galaxies [1]

Søren S. Larsen and Jean P. Brodie

UCO / Lick Observatory, UC Santa Cruz, USA

soeren@ucolick.org, brodie@ucolick.org

and

John P. Huchra

Harvard-Smithsonian Center for Astrophysics, USA

and

Duncan A. Forbes

Astrophysics & Supercomputing, Swinburne University, Hawthorn VIC 3122, Australia

and

Carl Grillmair

SIRTF Science Center, California Institute of Technology, USA

ABSTRACT

We present a study of globular clusters (GCs) in 17 relatively nearby early-type galaxies, based on deep F555W and F814W images from the Wide Field / Planetary Camera 2 (WFPC2) on board the Hubble Space Telescope (HST). A detailed analysis of color distributions, cluster sizes and luminosity functions is performed and compared with GCs in the Milky Way. In nearly all cases, a KMM test returns a high confidence level for the hypothesis that a sum of two Gaussians provides a better fit to the observed color distribution than a single Gaussian, although histograms of the $(V-I)_0$ distribution are not always obviously bimodal. The blue and red peak colors returned by the KMM test are *both* found to correlate with absolute host galaxy B band magnitude and central velocity dispersion (at about the $2-3\sigma$ level), but we see no clear correlation with host galaxy $V-I$ or $J-K$ color. Red GCs are generally smaller than blue GCs by about 20%. The size difference is seen at all radii and within sub-bins in $(V-I)_0$ color, and exists also in the Milky Way and Sombrero (M104) spiral galaxies. Fitting t_5 functions to the luminosity functions of blue and red GC populations separately, we find that the V-band turn-over of the blue GCs is brighter than that of the red ones by about 0.3 mag on the average, as expected if the two GC populations have similar ages and mass distributions but different metallicities. Brighter than the "turn-over" at $M_V \sim -7.5$, the luminosity functions (LFs) are well approximated by power-laws

with an exponent of about -1.75. This is similar to the LF for young star clusters, suggesting that young and old globular clusters form by the same basic mechanism. We discuss scenarios for GC formation and conclude that our data appear to favor "in-situ" models in which all GCs in a galaxy formed after the main body of the proto-galaxy had assembled into a single potential well.

Subject headings: galaxies:elliptical and lenticular,cD — galaxies:evolution — galaxies:star clusters

1. Introduction

Based on current observational evidence, swarms of globular clusters (GCs) appear to surround virtually all large galaxies and quite a few lesser ones. In particular, it was noted early on that large elliptical galaxies like e.g. M87 are hosts to exceedingly rich GC populations (Baum 1955). Before the advent of sensitive CCD detectors in the early 1980s, studies of GCs in galaxies beyond the Local Group remained very demanding, but over the past couple of decades an impressive amount of photometric data has been collected for globular clusters (GCs) in external galaxies. Further progress has been made with data from the *Hubble Space Telescope*, reducing contamination to a minimum because of its superior resolution.

Studies of extragalactic GCs have often aimed at characterizing the properties of all GCs around any given galaxy as a *system* and comparing these with the GC system of our own and other galaxies. Since GCs are generally thought to have formed very early, it has been anticipated that similarities and/or differences between GCSs in various galaxy types would eventually contribute to an improved understanding of the formation and early evolution of their host galaxies.

Perhaps the most celebrated of the similarities between GCSs in different galaxies is the apparently "universal" *luminosity function* of globular clusters. When plotted in magnitude units, the globular cluster luminosity function (GCLF) in practically all galaxies studied to date appears to be quite well fit by a Gaussian with a mean or "turn-over" at $M_V \sim -7.5$ and a dispersion of $\sigma_V \sim 1.2$ (Harris 1991; Ashman and Zepf 1998). However, few studies have reached deeper than ~ 1 mag below the turn-over and there have been plenty of attempts to fit Gaussians to even shallower data. It is also worth noting that there is no *a priori* reason to prefer a Gaussian as a fitting function. In the few galaxies where the luminosity distribution of globular clusters is known to several magnitudes fainter than the turn-over, other analytic functions actually provide a better fit. Secker (1992) found that in the Milky Way and M31, a t_5 function is a significant improvement

[1]Based on observations with the NASA/ESA Hubble Space Telescope, obtained at the Space Telescope Science Institute, which is operated by the Association of Universities for Research in Astronomy, Inc. under NASA contract No. NAS5-26555.

compared to a Gaussian. Although the difference between a Gaussian and a t_5 function is relatively minor when plotted in the standard magnitude space, it turns out to be very conspicuous when the LFs are plotted in *luminosity* units (Sect. 2).

In recent years, HST observations have revealed extremely luminous *young* star clusters in starburst environments. For any reasonable M/L ratios, these young clusters have masses that are easily within the range spanned by typical old globular clusters, and it is tempting to assume that the study of such clusters may tell a great deal about how the old GCs formed. The luminosity functions of young clusters generally follow power-law distributions of the form $n(L)dL \propto L^{\alpha}dL$. For young clusters in the "Antennae", Whitmore et al. (1999) found an overall LF slope of $\alpha = -2.6$ above $\sim 10^5 \mathrm{M}_{\odot}$ and $\alpha = -1.7$ below this limit. However, Zhang & Fall (1999) found that the *mass* function of Antennae clusters is well represented by a power law with exponent -2 over the entire mass range $10^4 < M < 10^6 \mathrm{M}_{\odot}$. For young clusters in the recent merger NGC 3256, Zepf et al. (1999) found a power-law with exponent -1.8 to be a good fit to the LF, and similar power-laws have been fitted to the LFs of massive young clusters in starburst galaxies like He 2–10 ($\alpha = -1.8 \pm 0.1$) and NGC 1741 ($\alpha = -1.9 \pm 0.1$) (Johnson et al. 1999, 2000). For Milky Way open clusters (van den Bergh & Lafontaine 1984) and young clusters in the LMC (Elson & Fall 1985), the LF is well represented by a power law with $\alpha \sim -1.5$. However, when evolutionary effects are taken into account the slope of the *mass* function may be closer to -2 (Elmegreen & Efremov 1997). The mass/luminosity functions for a variety of other young objects (e.g. HII regions and Giant Molecular Clouds) are generally well represented by similar power-laws (Harris & Pudritz 1994; Elmegreen & Efremov 1997).

Unfortunately, the fact that LFs of old globular clusters have traditionally been discussed as a function of *magnitude*, while studies of young cluster systems often use linear luminosity units, makes direct comparison of the LFs of young and old clusters more difficult. This has sometimes led to the misconception that the LFs of young and old clusters are dramatically different. However, the *upper* part of the LF of old GCs and the LF of young clusters are, in fact, well represented by power-laws with very similar exponents. For example, Kissler et al. (1994) and Kissler-Patig et al. (1996) found power-laws with a slope of $\alpha = -1.9 \pm 0.1$ to be a good fit to the mass function for old GCs brighter than the turn-over in the two ellipticals, NGC 4636 and NGC 720. Important clues to the formation of old GCs may lie in the similarity of their LF to that of young objects rather than in the differences, which become apparent mainly for luminosities *fainter than* the GCLF turn-over. Furthermore, little is actually known about the detailed behavior of the faint end of the GCLF, and in particular, whether the shape of the LF is really universal at the faintest levels in old as well as young cluster systems.

Another important result concerns the *color* distribution of old GCs. One of the more striking recent discoveries has been that of *bimodal color distributions* for GC systems (Elson & Santiago 1996; Geisler, Lee & Kim 1996; Kissler-Patig et al. 1997). This was originally predicted by Ashman and Zepf (1992) as a consequence of gas-rich mergers. In their scenario, a merger product would contain a metal-poor (blue) GC population inherited from the progenitor galaxies and a metal-rich

(red) population, formed in the merging process. After the initial excitement about the discovery of bimodal color distributions it has become clear that not all observed properties of GC systems fit into the merger picture and alternatives have been suggested (Forbes, Brodie and Grillmair 1997; Côté, Marzke and West 1998; Hilker et al. 1999). It is probably fair to say that there is currently no consensus concerning theories for the origin of multiple globular cluster populations within galaxies (Rhode & Zepf 2001), but bimodal color distributions have turned out to be very common (Gebhardt & Kissler-Patig 1999; Kundu 1999) and understanding them is bound to provide insight into processes that must have been common in the evolutionary history of galaxies.

In spite of the often-quoted strong evidence in favor of the "universal" GCLF, there may be some reason to question its universality. In a recent study of the nearby S0 galaxy NGC 1023, Larsen and Brodie (2000) found a number of clusters with much larger effective radii (about 10 pc) than normal GCs. Interestingly, these clusters were also *fainter* and did not fit a "standard" GCLF. It is also well-known that the outer, more extended halo clusters in the Milky Way are generally fainter and do not share the standard GCLF (van den Bergh 1983, 1996). This underscores the need to explore the *faint* end of the GCLF and test whether it is truly universal. Combining the photometric data with information about the sizes of individual globular clusters may provide further clues to the origin of GC systems, e.g. in order to check whether the faint extended clusters in NGC 1023 are a common phenomenon, or if they are unique to this galaxy and therefore presumably formed in some rare event.

In the Milky Way, globular clusters typically have half-light (effective) radii of about 3 pc (Harris 1996) although clusters in the outer halo are significantly larger (van den Bergh 1996). At the distance of the nearest large galaxy clusters (Virgo and Fornax), this corresponds to about $0\farcs04$, so whether these GC sizes are typical in other galaxies remained completely unknown until the HST era. Sizes of GCs beyond the Local Group have now been measured in a number of galaxies and it appears that GCs in other galaxies have roughly the same sizes as in the Milky Way. More surprisingly, it appears that the *red* GCs are generally somewhat smaller than the *blue* ones by 20 – 30% (Kundu and Whitmore 1998; Puzia et al. 1999; Kundu et al. 1999; Larsen and Brodie 2000). Whether this difference was set up at formation or is due to dynamical evolution remains an open question.

The HST archive now contains images of more than 50 early-type galaxies and thus provides an invaluable database for studying and comparing GCSs around different galaxies. Such surveys have already been undertaken by other authors (Gebhardt & Kissler-Patig 1999; Kundu 1999) and we do not intend to duplicate their efforts here. However, the previous studies have put their main emphasis on a comparison of as many GCSs as possible, not necessarily requiring homogeneity in depth and/or choice of bandpasses. Here we aim at a more specific investigation of relatively nearby galaxies for which *deep* HST WFPC2 imaging is available in the F555W and F814W bands, which can be accurately transformed to standard V and I magnitudes. Most of the data were obtained in Cycles 5 and 6 by our group, where much of the Cycle 6 data is published for the first time in this paper. We have supplemented our data with archive data, but only data with

exposure times comparable to those of our Cycle 5/6 datasets have been included in order to reach well beyond the GCLF turn-over and provide sufficient S/N for size measurements. We have also obtained photometry for objects in two comparison fields as a check of background/foreground contamination.

2. Analytic models of luminosity functions

As shown by Secker (1992), the Student's t_5 function

$$\frac{8}{3\sqrt{5}\pi\sigma_t}\left(1+\frac{(M-\mu_t)^2}{5\sigma_t^2}\right)^{-3} \tag{1}$$

where μ_t is the turn-over magnitude and σ_t is the dispersion of the t_5 function, provides a significantly better fit to the Milky Way and M31 GCLFs than a Gaussian. This is illustrated in the left panel of Fig. 1 which shows the Milky Way GCLF together with a Gaussian and a t_5 function, both with a mean of $M_V = -7.3$ and dispersions of $\sigma_G = 1.4$ and $\sigma_t = 1.1$ respectively (Secker 1992). The t_5 function evidently provides a better fit than the Gaussian, particularly at the faint end. However, if one restricts the fit to clusters brighter than $1-2$ mag below the turn-over, as in most studies of extragalactic GCSs, the difference remains quite subtle.

The difference between the Gaussian and the t_5 function becomes much more clear when plotting the number of clusters per *luminosity* bin rather than per *magnitude* bin, as illustrated in the right-hand panel of Fig. 1. In luminosity units, a log-normal distribution is actually quite far from providing a satisfactory fit below $\sim 10^4 \mathrm{L}_\odot$ or $M_V \simeq -5$, while the t_5 function does, in fact, match the observed luminosity function almost perfectly. Normalizing the two functions to the same value at the turn-over, the difference between the t_5 function and the Gaussian amounts to a factor of 4 at $M_V = -4$ and increases rapidly below this limit, reaching a factor of 30 at $M_V = -3$. So although the difference between a Gaussian and a t_5 function is almost indiscernible for typical extragalactic GC data, it becomes quite significant at faint levels. This difference may turn out to be of great relevance to the understanding of dynamical destruction processes in GC systems, as a t_5–like distribution requires considerably fewer low-mass clusters to be destroyed for an initially uniform power-law mass distribution.

In addition to Gaussian and t_5 functions, other analytical models have been used to fit the mass- and luminosity functions of globular clusters as well. Abraham & van den Bergh (1995) used Gauss-Hermite expansions to characterize the Galactic GCLF but found the higher-order terms to be small, indicating no strong deviations from a pure Gaussian. Baum et al. (1995) preferred a composite of two exponentials over Gaussian or t functions as a fit to the combined LF of Milky Way and M31 globular clusters, corresponding to two power-law segments if luminosity units are used instead of magnitudes. A figure comparing the Gaussian, t_5 and exponential functions is given in that paper. Two-component power-law fits were also used by Harris & Pudritz (1994) to fit the mass distribution of old globular clusters, and there is some evidence that the highest-mass clusters

may follow a third power-law mass distribution (McLaughlin, Secker, Harris & Geisler 1995).

3. Data

Basic data for the galaxies studied in this paper are listed in Table 1. The first column of the table gives the galaxy name. Some galaxies have two or more pointings, usually with one pointing centered on the galaxy nucleus and another one offset from the center, denoted by a '-O' suffix. The second column of Table 1 gives the name of the original principal investigator (PI) of the dataset, along with the ID (PID) of the proposal from which the data originate. Exposure times in sec in F555W and F814W are in cols. 3 and 4. A number of additional host galaxy parameters are given in Table 2, including infrared JHK colors from the 2MASS survey (Jarrett et al. 2000).

In three cases we have included data which are not in the F555W/F814W bands: Two galaxies in the Fornax cluster (NGC 1399, NGC 1404) were observed in F450W / F814W and data for the "Sombrero" galaxy (M104) is in F547M / F814W. While the latter is easily transformed to $V-I, V$ photometry, the NGC 1399 / NGC 1404 data is closer to the $B-I, B$ bands and will only be transformed to $V-I, V$ (using transformations in Forbes & Forte (2000)) when this is essential for comparison with the other galaxies.

We have generally included galaxies for which integrations longer than about 2000 sec were available in both F555W and F814W. However, for a few nearby galaxies (NGC 3115, NGC 3379, NGC 3384 and NGC 4594) this requirement has been relaxed. In all cases, the exposures listed in Table 1 actually consist of two or more shorter integrations.

The data were downloaded from the archive at STScI and initial reductions (flatfielding, bias subtraction etc.) were performed "on the fly" by the standard pipeline processing system. Subsequent reductions were done with IRAF[2] and closely followed the procedure described in Larsen and Brodie (2000). The individual exposures in each band were combined using the IMCOMBINE task, with the **reject** option set to **crreject** in order to eliminate cosmic ray (CR) hits. In most cases, the individual exposures images were well aligned so that no shifts were required before combination, but when shifts were necessary they were applied with the IMSHIFT task.

For the central pointings, a sky background subtraction was done. First, point sources were subtracted from the raw images using the `ishape` algorithm (Larsen 1999). The object-subtracted images were then smoothed with a 15×15 pixels median filter and the smoothed images were then subtracted from the original images, providing our final set of background-subtracted images for further analysis.

Photometry was done with the PHOT package within IRAF. Point sources were detected using

[2]IRAF is distributed by the National Optical Astronomical Observatories, which are operated by the Association of Universities for Research in Astronomy, Inc. under contract with the National Science Foundation

the DAOFIND task, but because of the varying S/N within the images it was necessary to impose further selection criteria in order to avoid spurious detections. This was done by measuring the noise level directly off the images in a small annulus around each object and only including objects which had a S/N higher than 3 within an aperture radius of 2 pixels in both F555W and F814W. Aperture photometry for all objects in the final object lists was then obtained using the APPHOT task. For the background-subtracted images a fixed background level of 0 was used, while the background was measured between 30 and 50 pixels from the object in the off-center pointings.

The transformation from F555W / F814W magnitudes to the standard $V, V-I$ system was done following the standard procedure as described in Holtzman et al. (1995). Charge-transfer efficiency corrections from Stetson (1998) were also applied, even though this correction is nearly negligible in our case because of the underlying galaxy light. We note that the recent recalibration of WFPC2 data reduced with HSTphot (Dolphin 2000) would cause $V-I$ colors to be redder by 0.02 mag compared to the Holtzman et al. calibration.

Colors were measured in an $r = 2$ pixels aperture, but because globular clusters are expected to appear as slightly extended sources in our images we decided to use a slightly larger $r = 3$ pixels aperture for V magnitudes. For colors the use of a smaller aperture is justified even for extended objects because the *difference* between aperture corrections in different bands is nearly independent of object size (Holtzman et al. 1996; Larsen and Brodie 2000). We have adopted aperture corrections from our science aperture to the Holtzman et al. $0\farcs5$ reference apertures of $\Delta V_{\rm WF} = -0.15$ mag and $\Delta(V-I)_{\rm WF} = 0.03$ mag for the WF chips and $\Delta V_{\rm PC} = -0.55$ mag and $\Delta(V-I)_{\rm PC} = 0.120$ mag for the PC chip, respectively. These aperture corrections are derived for objects that have King profiles with an effective radius of 3 pc and $r_{\rm tidal}/r_{\rm core} = 30$ at a distance of about 10 Mpc, typical for GCs in galaxies such as NGC 1023 and NGC 3115. At the distance of Virgo ($\sim$ 16 Mpc), GCs will have smaller apparent sizes and our magnitudes may thus be too bright by a few times 0.01 mag. However, colors are not affected. For a thorough discussion of aperture corrections and their dependence on object size we refer to Larsen and Brodie (2000).

In addition to the data listed in Table 1, we included two comparison fields to check contamination by foreground/background sources. One of these fields is located about 2 deg from the galaxy NGC 1023 (From HST proposal 6254, PI: E. Groth). The data for this field consist of 2×1300 sec in each of the F606W and F814W bands, i.e. roughly as deep as our science data. The other field is the *Hubble Deep Field* (HDF) (Williams et al. 1996) for which we combined F606W and F814W images to obtain total integration times of 6300 sec and 12900 sec in the two bands, respectively. Although the transformation of F606W/F814W data to standard $V, V-I$ photometry is presumably less accurate than for F555W/F814W data, it should be good enough for our comparison purposes.

Completeness tests were carried out by adding artificial objects to the science images and redoing the photometry. 500 artificial objects were added to each chip at random positions, but with required separations larger than 10 pixels in order to avoid crowding problems. The artificial

objects were added to the science images using the `mksynth` task (Larsen 1999), again generating the object profiles by convolution of King profiles similar to those used for the aperture corrections with the WFPC2 PSF as modeled by the `tinytim` program (Krist and Hook 1997). Here the King profiles were scaled according to the distances listed in Table 2. In principle, the completeness corrections will be color dependent, but GCs generally span a relatively narrow range in colors (typically between $(V-I)_0 = 0.8$ and 1.2) so for these tests we assumed constant object colors of $V-I = 1.0$, which is close to the average colors of GCs. The 50% completeness limit was generally found to be between $V = 25$ and $V = 26$, in most cases well below the expected turn-over of the globular cluster luminosity functions.

4. Description of galaxies

Our sample consists of 17 galaxies of which 1 is classified as type Sa, 4 are classified as S0, 11 are ellipticals and 1 is a cD. In the following we give a short description of each galaxy with references to earlier work pertaining to their GC systems.

NGC 524
This massive S0 galaxy dominates a small group. It has a relatively rich GC system with a specific frequency S_N (Harris and van den Bergh 1981) ~ 3.3 (Ashman and Zepf 1998). Here we detect a total of 617 GCs, second only to the cD galaxy NGC 4486 (M87).

NGC 1023
At 9.8 Mpc, NGC 1023 is the nearest S0 galaxy. It is the brightest galaxy in a group of 13 galaxies (Tully 1980). Its GC system has been studied recently using HST by Larsen and Brodie (2000). As well as the expected blue and red GC subpopulations, they identified a third subpopulation of red, spatially extended clusters. The origin of these extended clusters is currently unknown.

NGC 3115
This bulge–dominated S0 galaxy is also very nearby. It has a modest GC system, which has been examined using HST by Kundu and Whitmore (1998). They identified 144 GCs with a similar color distribution to that listed in Table 3. In addition they noted that the red GCs were smaller than the blue ones by ∼20%. Mainly because of our selection criteria, designed for somewhat more distant galaxies than NGC 3115 and therefore with a brighter lower magnitude limit, we detect fewer GCs in NGC 3115 than Kundu and Whitmore (1998).

NGC 3379
Also known as M105, NGC 3379 is the dominant elliptical in the nearby Leo group. Along with NGC 3377, it has a relatively low specific frequency, i.e. $S_N \sim 1.2$ (Ashman and Zepf 1998). Here we detect only 55 GCs with bimodality likely, but not certain.

NGC 3384
Also in the Leo group, this S0 galaxy has $S_N \sim 0.9$ (Ashman and Zepf 1998). We detect a total of

54 GCs, of which 30 formally fall in the "blue" category and 24 in the red, but with no statistical evidence for bimodality.

NGC 4365

Probably located slightly behind the Virgo cluster, this large elliptical contains a kinematically distinct core (Bender 1988) which may indicate a past merger event. The first HST study was that of Forbes et al. (1996). From a short exposure, central pointing they detected 328 GCs but no obvious bimodality. Here we use longer exposure images of the galaxy center and a region directly to the north. We find a broad color distribution for 323 clusters brighter than $V = 24$, although most GCs seem to belong to a peak with the same color as the blue population in most large ellipticals.

NGC 4406

This luminous early-type (E3/S0) Virgo galaxy is also known as M86. It is a rare example of an early type galaxy with an X-ray plume, presumably resulting from ram pressure stripping (Rangarajan et al. 1995). A kinematically distinct core was found by Bender (1988). It was part of the same HST study by Forbes et al. (1996) which included NGC 4365. Like NGC 4365, no obvious bimodality was detected in the short exposure images. Kundu (1999) found tentative evidence for bimodality with peaks at $(V-I)_0$= 0.98 and 1.17; here we formally find peaks at $(V-I)_0 = 0.986$ and 1.145 but still with bimodality detected at a low confidence level.

NGC 4472

Also known as M49, this galaxy is the most luminous in the Virgo cluster, dominating its region of the subcluster. It has a joint elliptical and S0 classification and a kinematically distinct core (Davies & Birkinshaw 1988). NGC 4472 has been the subject of numerous GC studies and contains perhaps the best characterized GC system of any early–type galaxy. Spectroscopic studies (Bridges et al. 1997; Beasley et al. 2000; Zepf et al. 2000) have determined the mean metallicity of the GC system and begun to constrain the age and kinematics. Photometric studies (Lee et al. 1998; Puzia et al. 1999; Lee & Kim 2000; Rhode & Zepf 2001) have detected large numbers of GCs with clear evidence for bimodality. In terms of the peak colors, there are slight differences between our results and the other HST studies even though all three use essentially the same data set. We find $(V-I)_0$ = 0.94 and 1.21, which is consistent with the findings of Lee & Kim (2000) and Puzia et al. (1999) after extinction corrections. We also confirm that the turn-over magnitude of the red GCs is fainter than for the blue GCs, as noted by Puzia et al. (1999).

NGC 4473

This is a highly elongated Virgo elliptical. Kundu (1999) reports bimodality from HST data. Our detection of bimodality is statistically not compelling, but we find similar mean color peaks to Kundu.

NGC 4486

As the Virgo central elliptical galaxy (M87) it lies at the center of the Virgo cluster gravitational potential and X–ray emission, although it is moving slightly with respect to the cluster center of

mass velocity as determined from galaxy velocities (Huchra 1985). Its GC system is exceptionally rich with over 10,000 GCs and a $S_N \sim 14$ (Ashman and Zepf 1998). HST observations have allowed the bimodality to be well defined (Elson & Santiago 1996). Spectroscopic studies have derived metallicities and kinematics for a large number of M87 GCs (Mould, Oke & Nemec 1987; Huchra & Brodie 1987; Cohen et al. 1998).

NGC 4494
Located in the Coma I cloud, this elliptical contains a kinematically distinct core (Bender 1988). From HST data, Forbes et al. (1996) suggested a low specific frequency of $S_N \sim 2$. The same HST data suggested mean color peaks around $(V-I)_0 = 0.95$ and 1.15, here we find 0.92 and 1.12.

NGC 4552
This Virgo elliptical is also known as M89, and is known to posses a kinematically distinct core (Simien & Prugniel 1997). Kundu (1999) found possible bimodality, which we confirm as statistically significant with the same mean colors (to within $\pm$ 0.01).

NGC 4594
Known as 'The Sombrero' (M104), it is the closest Sa type galaxy. With an exceptionally large bulge/disk ratio of ~ 6 (Kent 1988), it represents an intermediate case between ellipticals and early type spirals. Its GC system is perhaps the most populous system of any spiral galaxy with 1200 $\pm$ 100 estimated by Harris et al. (1984). Photometry (Forbes et al. 1997) and spectroscopy (Bridges et al. 1997) of the GC system indicates a mean metallicity similar to that for elliptical galaxies. Recently, Larsen, Forbes & Brodie (2001) have utilized three HST pointings of M104 to conduct a detailed study of the GC system. They detected strong color bimodality, and found the red GCs to be $\sim$30% smaller than the blue ones. The Sombrero data used in this study are the same as those used by Larsen, Forbes & Brodie (2001).

NGC 4649
Another giant Virgo elliptical (known as M60), with $S_N \sim 6.7$ (Ashman and Zepf 1998). Both ourselves and Kundu (1999) detect clear bimodality.

NGC 4733
This galaxy is a low luminosity Virgo elliptical. We detect only 28 GC candidates, too few to draw conclusions about bimodality although most clusters appear to belong to a blue peak.

NGC 1399
Although of rather modest optical luminosity, NGC 1399 is the central elliptical galaxy of the Fornax cluster. It has around 5000 GCs giving it a high specific frequency (Bridges et al. 1991). Studies of the kinematics of the NGC 1399 GC system have been carried out by Grillmair et al. (1994) and Kissler-Patig et al. (1998). Here we use the same B and I band HST data of Grillmair et al. (1999), but convert the color peaks to $V-I$.

NGC 1404
This galaxy lies within the X–ray envelope of NGC 1399, and may be losing GCs to it. Also part

of the Forbes et al. (1998) and Grillmair et al. (1999) photometric studies, we confirm a bimodal color distribution with about the same peaks as for the GCs in NGC 1399.

5. Results

5.1. Color-magnitude diagrams

Color-magnitude diagrams (CMDs) for objects in the 17 galaxies in our sample are shown in Fig. 2. Typical errors in $V-I$ are indicated by the error bars at $(V-I)_0 = 2.0$. Note that the CMDs for NGC 1399 and NGC 1404 are in $(B-I)_0, B$ units, although the magnitude and color ranges shown for these galaxies have been scaled to match those of the $(V-I)_0, V$ plots. The horizontal dashed lines indicate approximate 50% completeness limits from the completeness tests. As mentioned above, these completeness limits are for objects with typical GC sizes and colors; objects with larger sizes will have brighter 50% completeness limits. Note, however, that we reach well below the expected GCLF turn-over at $M_V \simeq -7.5$ ($M_B \simeq -6.8$) in all galaxies.

The GC sequences are easily recognizable in Fig. 2, extending over nearly the entire plotted magnitude range and with colors between $(V-I)_0 \simeq 0.8$ and $(V-I)_0 \simeq 1.25$ (the blue objects in the NGC 4649 field with $(V-I)_0 < 0.5$ actually belong to the nearby spiral galaxy NGC 4647, located $2\farcm5$ from NGC 4649). Although some CMDs exhibit strikingly bimodal color distributions (e.g. NGC 1023, NGC 1404, NGC 4472 and NGC 4649) and others show less evidence for two distinct peaks in the $V-I$ colors, the *total range* in $(V-I)_0$ spanned by the GC sequence is always much larger than the photometric errors. For further analysis, globular cluster (GC) candidates were selected within the color range $0.70 < (V-I)_0 < 1.45$ ($-2.2 <$ [Fe/H] < 0.2) and individually adjusted magnitude limits, as indicated by the boxes superimposed on the CMDs in Fig. 2.

Fig. 3 shows the CMDs for the two comparison fields. The HDF appears to contain more objects than the other comparison field, perhaps partly as a consequence of the much longer exposures which make it easier to detect extended sources. Comparing Fig. 3 and Fig. 2, we see that contamination is unlikely to pose much of a problem for the richer GCSs. However, for the poorer systems one obviously needs to carefully address the contamination issue.

5.2. Color distributions and bimodality

In order to make more quantitative statements about bimodality, a KMM test (Ashman, Bird & Zepf 1994) was applied to the data. To reduce photometric errors, only clusters brighter than 1.0 mag above the lower magnitude limit indicated by the boxes in Fig. 2 were included. The KMM test uses a maximum-likelihood technique to estimate the probability that the distribution of a number of data values (in this case the $V-I$ colors of GCs) is better modeled as a sum of two Gaussians than as a single Gaussian, as indicated by the number $1-P$. Here we have used a homo-

scedastic test, i.e. the two Gaussians are assumed to have the same dispersion. The KMM algorithm also supports heteroscedastic fits (different dispersions) but these tend to be more unstable and are generally not recommended unless there are strong reasons to expect that the dispersions are significantly different (Ashman, Bird & Zepf 1994).

Table 3 lists the colors of the two peaks, the P value, and the numbers of clusters assigned to each peak by KMM. Fig. 4 shows histograms for the $(V-I)_0$ colors of the GCs fitted by the KMM test, together with Gaussians corresponding to the two color peaks and their sum. In spite of the visual impression that many of the color distributions may not be convincingly bimodal, the P value is actually close to 0 in nearly all cases, indicating a high probability that two Gaussians are a better fit than a single one. Furthermore, the KMM test returns consistent $(V-I)_0$ peak colors even in galaxies where the CMDs and $(V-I)_0$ histograms show weak or no evidence of bimodality. However, we note that NGC 4365 does appear to have only one peak, centered on $(V-I)_0 = 0.98$. Thus, the GCs in this galaxy have colors typical for the blue (metal-poor) populations in the bimodal systems, while the red GC population seems to be largely absent.

The average colors of the blue and red peaks are $(V-I)_0 = 0.95$ and $(V-I)_0 = 1.18$, with a scatter of about 0.02 mag and 0.04 mag for the two peaks, respectively. The $(V-I)_0$ colors can be converted into metallicities e.g. using the calibration in Kissler-Patig et al. (1998), yielding [Fe/H] $= -1.4$ and [Fe/H] $= -0.6$. These metallicities are roughly similar to those of the metal-poor (halo) and metal-rich (disk/bulge) clusters in the Milky Way (Zinn 1985) and in M31 (Barmby et al. 2000). The relation given in Kundu and Whitmore (1998) leads to almost exactly the same metallicity for the blue peak and a somewhat higher metallicity of [Fe/H] $= -0.3$ for the red peak.

Of course, there is no *a priori* basis for the assumption that Gaussian functions are the best possible representation of the data. One may even dispute that a low P value is necessarily an indicator of bimodality *per se*, since any observed distribution that is broadened relative to a Gaussian distribution will generally result in a low P value. An alternative test for bimodality is the so-called "DIP statistic" (Hartigan & Hartigan 1985; Gebhardt & Kissler-Patig 1999) which measures the probability that a distribution is not unimodal, without any underlying assumptions about the details of the distribution. DIP values are listed in the last column of Table 3. The DIP probabilities are generally high for those color distributions that also visually appear to be strongly bimodal (e.g. NGC 1023, NGC 4649, NGC 4472, NGC 4486), and conversely, galaxies like NGC 524 and NGC 4365 have low DIP values.

5.3. Turn-over magnitudes

Several recent studies have found significant differences between the turn-over magnitudes for the LFs of blue and red GCs, with the blue GCs generally being brighter by a few tenths of a magnitude in the V band (Elson & Santiago 1996; Kundu et al. 1999; Puzia et al. 1999; Larsen and Brodie 2000). For a constant globular cluster *mass* distribution and similar ages, a

difference in turn-over magnitudes is an expected consequence of the variation in mass-to-light ratio with metallicity. For two equally old GC populations with metallicities of [Fe/H] = −1.4 and [Fe/H] = −0.6 and similar stellar IMFs, Ashman, Conti & Zepf (1995) find that the difference in V band magnitude amounts to about 0.22 mag. We also estimated mass to light ratios for simple stellar populations with [Fe/H] = −1.4 and [Fe/H] = −0.6 using 1996 versions of the Bruzual & Charlot population synthesis models and found an expected difference of 0.26 mag in the V-band turn-over magnitudes for two populations of similar old ages (12 – 15 Gyr). It should be noted that the dependence of mass-to-light ratio on metallicity is wavelength dependent and becomes weaker at longer wavelengths.

In the following we will refer to "blue" and "red" GC candidates as clusters with $(V-I)_0 < 1.05$ and $(V-I)_0 \geq 1.05$, respectively. The $(V-I)_0$ cut corresponds to a metallicity of [Fe/H] = −1.1 (Kissler-Patig et al. 1998) and is close to the natural division between halo and disk/bulge GCs in the Milky Way (Zinn 1985). We performed maximum-likelihood fits of t_5 functions (Secker 1992) to the luminosity distributions of our blue and red GC candidates, selected within the boxes in Fig. 2. Completeness corrections were done on a by-chip basis and a correction for contamination was performed by a statistical subtraction of objects in the NGC 1023 comparison field from the source lists. As a check of the maximum-likelihood fits, we also fitted Gaussian functions directly to histograms of the raw luminosity functions in a few cases, using the NGAUSSFIT task in the STSDAS package. The GCLF turn-over peaks estimated by the two methods typically agreed within about 0.15 mag, which is quite satisfactory considering that the Gaussian fits were performed on data that were corrected neither for completeness effects nor contamination.

To test how different completeness functions for blue and red GCs might affect the turn-over magnitudes, we carried out additional completeness tests for objects with $V-I = 0.8$ and $V-I = 1.2$ in two fields (one off-center pointing in NGC 4472 and the central pointing in NGC 4486). The t_5 function fits were then repeated for all combinations of GC subpopulations and completeness functions. Being at the extremes of the GC color distribution, these tests provide a worst-case estimate of how much color-dependent completeness corrections might affect the turn-over differences between blue and red GC populations. Regardless of the choice of completeness functions, the turn-over magnitudes remained constant to within 0.05 mag.

The results of our maximum-likelihood fits are listed in Tables 4 and 5 for blue and red subpopulations separately, as well as for the combined samples. The last column of each table lists the difference $\Delta m_V^{\rm TO}$ between the turn-over magnitudes of the blue and red GC populations in each galaxy. In Table 4, both the dispersion (σ_t) and turn-over were fitted, while the dispersion was kept fixed at $\sigma_t = 1.1$ in Table 5. This dispersion corresponds to the value reported for the Milky Way GCS by Secker (1992).

Indeed, we find that the blue GCs are generally brighter than the reds by typically a few times 0.1 mag. The difference is significant in all galaxies, including those without obviously bimodal color distributions (e.g. NGC 524, NGC 4365). In particular, we confirm the offset between the

turn-over magnitudes of the two GC populations in NGC 4472 which was first reported by Puzia et al. (1999), but subsequently claimed not to exist by Lee & Kim (2000) based on essentially the same data. Averaging all the $\Delta m_V^{\rm TO}$ values in Table 4 and weighting each value inversely by the sum of its positive and negative errors yields a mean difference between the turn-over of the red and blue GC populations of 0.47 mag. Within the uncertainties, all $\Delta m_V^{\rm TO}$ values in the table are consistent with this number, which is somewhat larger than the prediction by population synthesis models. It is perhaps worth noting that a few galaxies show much larger $\Delta m_V^{\rm TO}$ values than the typical ~ 0.5 mag, even though the formal errors on $\Delta m_V^{\rm TO}$ are also larger than average in those cases. In particular, the two galaxies NGC 1023 and NGC 3384 both have $\Delta m_V^{\rm TO} > 1$. These two galaxies both appear to contain a third population of clusters which are intrinsically fainter than 'real' globular clusters and predominantly red (Larsen and Brodie 2000, see also Sect. 5.4 and 5.5.1) and may be responsible for shifting the fit for the red GCs towards fainter magnitudes. If NGC 1023 and NGC 3384 are excluded the average $\Delta m_V^{\rm TO}$ value decreases to 0.40 mag with a scatter of ± 0.24 mag.

If we use the fixed-σ_t fits in Table 5 instead of the two-parameter fits in Table 4 and again exclude NGC 1023 and NGC 3384, the average $\Delta m_V^{\rm TO}$ value decreases slightly to 0.37 mag with a scatter of ± 0.20 mag. Note that the $\Delta m_V^{\rm TO}$ values for NGC 4472 and NGC 4365, which were in both cases larger than 0.80 mag for the two-parameter fits, now decrease to 0.50 mag and 0.56 mag, respectively. However, for NGC 1023 and NGC 3384 the $\Delta m_V^{\rm TO}$ values remain unusually large also for the one-parameter fits.

Although one may potentially obtain a better fit to the data by letting the dispersion vary, the two-parameter fits are also more sensitive to outlying data points, inaccurate contamination and/or completeness corrections etc. It is therefore not surprising that the scatter in $\Delta m_V^{\rm TO}$ decreases when only one parameter (the turn-over magnitude) is fitted, and it seems reasonable to assume that the one-parameter fits yield somewhat more accurate estimates of the turn-over magnitudes, especially for the cluster-poor GC systems. This should certainly be the case if the GCLF is truly universal, with a (nearly) constant dispersion from galaxy to galaxy. If the sample is further restricted to galaxies for which the errors (average of positive and negative) on $\Delta m_V^{\rm TO}$ are < 0.25 mag, then we get an average $\Delta m_V^{\rm TO} = 0.30$ for both one- and two-parameter fits, with a scatter of ± 0.16 mag in both cases. Of course, selecting the galaxies by the errors on the t_5 fits introduces a bias towards cluster-rich systems, which might have systematically different properties from the poorer GC systems, so whether or not the decrease in $\Delta m_V^{\rm TO}$ for the error-selected sample is real is hard to tell. In any case, the average $\Delta m_V^{\rm TO}$ values are quite close to the theoretical expectation for two GC populations of similar ages and mass distributions, but different metallicities.

In Table 5 we have also included t_5 function fits to Milky Way globular clusters (from Harris 1996). Following Secker (1992), we have only included clusters between 2 kpc and 35 kpc from the Galactic center and with color excess $E(B-V) < 1.0$. We exclude clusters fainter than $M_V = -5$, roughly corresponding to the magnitude limit in the other galaxies in our sample. These selection criteria leave only 67 "blue" ([Fe/H] < -1) and 20 "red" ([Fe/H] ≥ -1) clusters, so we decided not

to attempt two-parameter fits for these data. From one-parameter fits to the Milky Way data we find that the turn-over of the blue GCs is brighter than that of the red ones by $\Delta m_V^{\rm TO} = 0.46^{+0.34}_{-0.38}$ mag, which is similar to the average $\Delta m_V^{\rm TO}$ value for the other galaxies in the sample within the uncertainties. It is also of interest to compare with the GC system of M31: Curiously, Barmby et al. (2001) found that the metal-poor (blue) globular clusters in M31 are on average 0.36 *fainter* in V than the metal-rich (red) ones, a difference of about the same magnitude but opposite sign compared to most other GC systems. Barmby et al. (2001) argue against any possible selection effects as the cause of the measured GCLF differences in their sample, but note that independent confirmation using a more complete and less contaminated M31 cluster catalog would be highly desirable.

However, it is worth reiterating that a comparison of the GCLF turn-over magnitudes for different GC populations only makes sense for strictly identical *mass* distributions of the various populations. Establishing the mass distributions of GCs in external galaxies independently of the luminosities will be a very difficult task observationally. If the two populations did, in fact, form at different epochs in different environmental conditions, then one might indeed *expect* their mass functions to be different – especially considering that the mass function of clusters in present-day starbursts deviates from that of old GCs in the critical region near and below the GCLF turn-over. We therefore feel that it would be premature to draw further conclusions about age differences between GC subpopulations, based only on differences in the GCLF turn-over.

5.4. Luminosity functions

In Fig. 5 we show the luminosity functions for GCs in each of the 15 galaxies with V, I photometry. We use luminosity units rather than magnitudes; for this reason the familiar "Gaussian" shape of the GCLF is not apparent in the figure. The GCLF turn-over magnitude of $M_V = -7.5$ corresponds to about $8 \times 10^4\,{\rm L}_\odot$. For comparison, we have also included the LF for Milky Way globular clusters (shown with dots), using data from Harris (1996). The solid lines represent the raw LFs of GCs in each galaxy, uncorrected for completeness and/or contamination effects, while the two dashed lines in each plot represent the LF corrected for incompleteness and background contamination, using each of the two reference fields. For the HDF, the contamination correction was performed *after* completeness correction, since the HDF data are much deeper than any of our GC data. For the other comparison field we applied the contamination correction *before* correction for incompleteness. The HDF is somewhat richer in background galaxies than the field near NGC 1023, while the latter is located at lower galactic latitude ($b = 19\,{\rm deg}$) and thus presumably contains more Galactic foreground stars. The difference between the two dashed curves is likely to provide a rough indicator of the accuracy by which the LFs can be determined. The average 50% completeness limits are indicated by vertical dashed lines.

In order to compare with the LFs of young cluster systems, we performed power-law fits to the LFs of our GC data in the interval $10^5 < L < 10^6\,{\rm L}_\odot$ for red and blue clusters separately, and for

the combined sample (Table 6). In contrast to t_5 function or Gaussian fits where both the dispersion and mean can vary, power-law fits to the brighter portion of the LF are completely independent of the behavior of the data below the turn-over and therefore hardly affected by completeness effects. The numbers in Table 6 are for the raw data, i.e. not corrected for completeness or contamination. Applying these (uncertain) corrections changes the exponents by at most a few times 0.01. A weighted mean of data with errors on the power-law exponents less than 0.5 gives exponents of -1.66 ± 0.03 and -1.80 ± 0.06 for the blue and red clusters, respectively, and -1.74 ± 0.04 for the combined sample. These values are in very good agreement with those reported for a variety of *young* cluster systems (see the Introduction). The slight difference between the fits to the red and blue clusters is most likely due to the differences in the turn-over magnitudes of the two populations.

There are a few galaxies in which the *faint* end of the LF deviates significantly from that observed in the Milky Way. The most striking example is NGC 1023 which exhibits a strong excess of faint clusters (Larsen and Brodie 2000), readily visible by inspection of the color-magnitude diagram (Fig. 2), where especially the red GC sequence is seen to extend to very faint magnitudes. A similar effect is seen in NGC 3384, and also the Sombrero, NGC 4472, NGC 4365 and NGC 4649 may show a hint of this phenomenon although incompleteness and contamination problems at the faint end of the GCLF make the results less conclusive for these galaxies. Nevertheless, there might be reason to suspect that the GCLF is not as universal as previously thought and it would be desirable to have even deeper HST data for some of these galaxies. Variations from galaxy to galaxy at the faint end of the GCLF would have strong implications for theories for the formation and evolution of GC systems.

5.5. Sizes

The spatial resolving power of HST allows sizes of extragalactic GCs to be measured. Some recent studies have shown a general trend for the red clusters to be somewhat smaller than the blue ones, both in elliptical galaxies like NGC 4472 and M87 (Puzia et al. 1999; Kundu 1999), in S0 galaxies such as NGC 3115 and NGC 1023 (Larsen and Brodie 2000; Kundu and Whitmore 1998) and even in the Sa-type galaxy M104, the "Sombrero" (Larsen, Forbes & Brodie 2001).

Here we discuss in some detail the size distributions of GCs in our sample of galaxies. Because of the undersampling of the point spread function (PSF) by especially the WF cameras, it is necessary to take special care in avoiding instrumental effects. Here we have used the `ishape` algorithm (Larsen 1999) which models the cluster images as an analytic model profile convolved with the HST point-spread function, iteratively adjusting the model until the best possible match with the data is obtained. We have chosen King profiles (King 1962) with a concentration parameter of $c = 30$ (tidal / core radius) for the analytic models. Since the total integrated luminosity of King profiles is finite, the FWHM values measured by `ishape` can easily be converted to half-light (effective) radii ($R_{\rm e}$). All internal computations by the algorithm are performed on $10\times$ subsampled image arrays, except for a final convolution with the so-called "diffusion kernel" (Krist and Hook

1997). For the size measurements we use our F555W images, for which the diffusion kernel is best understood.

For the two off-center pointings in NGC 4472 and the central pointing in NGC 4365, the individual exposures had to be shifted before combination, inevitably altering the PSF and potentially causing systematic errors in the size measurements. In these cases, sizes were therefore measured separately on each of the raw exposures and then averaged. This also allowed us to obtain an estimate of the accuracy of the size measurements, by computing the rms deviation of the difference between sizes of clusters measured on the two sets of images. This test indicates an rms scatter of about 1.0 pc for the cluster sizes measured on individual exposures (assuming Virgo distance) down to $V = 23.5$. Sizes measured on combined images (either directly or by averaging two measurements) should therefore be accurate to about 1.0 pc down to $V = 24$ and in the following we adopt this magnitude limit for the size measurements.

Possible systematic effects in the size measurements, resulting from the choice of a particular fitting function, are discussed in Larsen (1999). Briefly, the *effective* radius is quite independent of the choice of fitting function as long as the sources have comparable sizes to the PSF (as in our case).

5.5.1. GC size versus color

Fig. 6 shows the GC sizes as a function of $(V-I)_0$ color ($(B-I)_0$ color for NGC 1399 and NGC 1404) while Fig. 7 shows histograms for the size distributions of red and blue clusters separately. The median sizes are listed in Table 7, which also gives cluster sizes in four narrower bins. In order to minimize the effect of "outliers" with abnormally large sizes, the median sizes in Table 7 are based on clusters with $R_{\rm e} < 10$ pc only. For comparison, Table 7 also includes data for GCs in the Milky Way (Harris 1996). For the Milky Way GCs, the division between "red" and "blue" clusters has been taken to be at [Fe/H]$=-1$.

Figs. 6 and 7 confirm that, in most cases, blue clusters are larger than red ones by typically $\sim 20\%$. In particular, this is true also for the two spiral galaxies in the table, i.e. the Sombrero and the *Milky Way*. There are a few notable exceptions where blue and red clusters appear to have similar sizes, including NGC 4365 and NGC 4552, although the size difference is often recovered when the reddest sub-bin ($1.20 < (V-I)_0 < 1.45$) is excluded.

As discussed by Larsen and Brodie (2000), the S0 galaxy NGC 1023 contains a population of extended, red clusters which are generally fainter than the "normal" compact, globular clusters. These "faint fuzzies" are clearly visible in Fig. 6, with sizes around 10 pc and a $(V-I)_0$ color of about 1.2. They are responsible for much of the excess of faint clusters relative to the Milky Way GCLF seen in Fig. 5 (Larsen and Brodie 2000). Among the remaining galaxies in our sample, a similar population of extended red objects appears to exist in NGC 3384. Apart from the generally poorer GCS of this galaxy, the appearance of its $(V-I)_0, R_{\rm e}$ diagram mimics that of NGC 1023.

Furthermore, as mentioned in Sect. 5.4, the GCLF of NGC 3384 shows an excess of faint clusters very reminiscent of that in NGC 1023. We thus suggest that NGC 3384 is the *second case* of a galaxy which hosts a population of these, hitherto unknown, extended red faint clusters.

Unfortunately, since the "faint fuzzies" are generally fainter than the GCLF turn-over, they are at the limit of reliable size measurements in the more distant galaxies in our sample. Furthermore, their extended nature and low surface brightness make their very detection more difficult than for "normal" compact GCs. It is therefore difficult to tell how common such objects are and deep HST imaging of more nearby galaxies would be highly desirable. Of the four galaxies in our sample where the faint extended clusters are readily detectable (NGC 1023, NGC 3115, NGC 3379 and NGC 3384), they are apparent in two and not detected in the other two. In particular in NGC 3115, with its relatively rich GCS and adequately deep photometry, there is little chance that a population of extended red clusters could have been overlooked.

In Fig. 8, the median GC sizes are plotted for each of the four $V-I$ sub-bins in Table 7 with symbol sizes proportional to the logarithm of the number of clusters. For easier comparison, cluster sizes have been normalized to 1.0 in the $0.90 < (V-I)_0 < 1.05$ bin (which typically contains the largest number of GCs). Note that the scatter in the GC sizes is much larger in the reddest bin. Interestingly, the cluster sizes decrease as a function of $V-I$ for the three bluest bins, but then tend to increase somewhat again in the reddest bin. In some galaxies like NGC 1023 and NGC 3384, this effect is possibly due to the "faint extended" clusters which have preferentially red colors while the cause is less obvious in other galaxies.

5.6. Trends with galactocentric distance

Correlations between cluster properties and distance from the center of their host galaxies can potentially provide further clues to the formation and evolution of the cluster systems. In this respect, HST studies are generally limited by the relatively small field of view: at the distance of Virgo, a WFPC2 exposure centered on the galaxy nucleus will reach out to about 8 kpc. For more distant galaxies the coverage obviously improves, but with the trade-off of decreased ability to measure cluster sizes. Here we will carry out a "case study" of three cluster-rich galaxies (NGC 4365, NGC 4472 and NGC 4486) in the Virgo cluster, all with more than one WFPC2 pointing.

Table 8 lists the sizes of blue and red clusters, colors of the blue and red peaks and numbers of blue and red clusters as a function of galactocentric distance R_g for these three galaxies. Here clusters are defined as "blue" or "red" with respect to the color cut at $(V-I)_0 = 1.05$. Sizes for individual clusters and peak colors were measured in the same way as described in the previous sections.

None of the galaxies shows any significant color gradients for either the blue or red peak. However, when plotting the ratio of blue to red clusters $N_{\rm blue}/N_{\rm red}$ as a function of R_g, both NGC 4486 and NGC 4472 show an increase in this ratio outwards (Fig. 9). In NGC 4486 the

increase in $N_{\rm blue}/N_{\rm red}$ is quite dramatic and almost certainly responsible for the color gradient reported by earlier studies (Strom et al. 1981; Lee and Geisler 1993; Cohen et al. 1998; Harris et al. 1998). A similar conclusion was reached by Kundu et al. (1999) for the central parts of NGC 4486. In NGC 4472 the trend in $N_{\rm blue}/N_{\rm red}$ vs. R_g is more subtle and mostly driven by the outermost bin, in good agreement with the analysis by Puzia et al. (1999) who concluded that the relative numbers of blue and red clusters in NGC 4472 change by no more than about 10% within the central $250''$. However, further out in the halo NGC 4472 shows a stronger decline in the number of red GCs (Geisler, Lee & Kim 1996). NGC 4365 actually shows a *decrease* in the $N_{\rm blue}/N_{\rm red}$ ratio outwards, although a slope of 0 is nearly within the error bars. It thus appears that the colors (and, by inference, metallicities) of GC subpopulations are largely *independent* of distance from the galaxy center. Any overall gradients seem to result only from a change in the mix of the subpopulations.

Concerning overall size trends as a function of R_g, only NGC 4365 shows a clear increase in the cluster sizes in the outermost regions. Apart from this, the GC sizes appear to be fairly constant in all the galaxies, and in particular the size *difference* between blue and red GCs in NGC 4472 and NGC 4486 persists at all radii. This same conclusion was reached for NGC 4472 by Puzia et al. (1999), although they did not estimate the absolute linear size of the GCs, and by Kundu et al. (1999) for the inner regions of NGC 4486.

In summary, the observable GC properties (colors, sizes) appear to be nearly independent of position within the galaxies, at least in the three large ellipticals studied here. Any changes in the average properties of GCs result primarily from different mixtures of the two populations. Unless the orbits of blue and red GCs are dramatically different, the mechanism that was responsible for their size difference must have operated with equal efficiency at all radii.

5.7. Sizes of globular clusters in the Milky Way

As noted in Sect. 5.5, globular clusters in the Milky Way show the same correlation between size and color as in other galaxies (Table 7). This is also illustrated in Fig. 10 where the effective radii are plotted as a function of metallicity and in Fig. 11 which shows the size distributions for metal-rich and metal-poor Milky Way globulars (dividing at [Fe/H] $= -1$). The two plots are very similar to those for extragalactic GCs in Figs. 6 and 7.

As in the other galaxies in our sample, the correlation between GC size and metallicity is also preserved when subdividing the metal-poor and metal-rich GC populations in the Milky Way. The median sizes of Milky Way globular clusters in the intervals [Fe/H] < -1.5, $-1.5 <$ [Fe/H] < -1, $-1.0 <$ [Fe/H] < -0.5 and $-0.5 <$ [Fe/H] are 3.28 pc, 3.00 pc, 2.48 pc and 2.06 pc, respectively. However, since the metal-poor (large) GCs are preferentially found at large galactocentric distances, it is hard to say whether the size-metallicity correlation follows from the size-R_g correlation, or vice versa. One way to approach this question would be to look at metal-poor and metal-rich clusters

occupying the same volume of space, although this would still not exclude the possibility that the different populations might have different orbital characteristics. Another problem is one of pure statistics – with a total of 147 known Milky Way GCs, sub-samples of GCs quickly become very small.

Table 9 lists the sizes of Milky Way GCs in three radial bins: $0 < R_g < 2$ kpc, $2 < R_g < 5$ kpc and $5 < R_g < 10$ kpc. Although the numbers of clusters in each bin are small, the table suggests that the size difference between metal-rich and metal-poor GCs also exists at all radii in our Galaxy. However, as in the ellipticals, further information about the orbits of individual clusters is necessary to tell whether or not the size difference could be due to dynamical processes.

6. Discussion

6.1. Correlations with host galaxy parameters

A relation between GC mean metallicity and parent galaxy luminosity was first suggested by van den Bergh (1975) and subsequently supported by spectroscopic work (Brodie & Huchra 1991). With the discovery of multiple GC populations, an obvious question is whether the GC metallicity vs. host galaxy luminosity and other relations are present for both red and blue GCs, for only one population, or if the observed mean relations might even result just from different mixtures of two populations with roughly constant metallicities. Previous attempts to address this question (e.g. Forbes, Brodie and Grillmair 1997; Burgarella, Kissler-Patig & Buat 2001) have generally been based on compilations of literature data, lacking homogeneity in the choice of filter systems, data reduction procedures etc. Here we reinvestigate correlations between properties of GC subpopulations and their host galaxies, based, for the first time, on a large homogeneous dataset.

In Fig. 12 the $(V-I)_0$ colors of the two GC subpopulations returned by the KMM test (Table 3) are shown as a function of the various host galaxy parameters listed in Table 2: absolute B magnitude, central velocity dispersion, $(V-I)_0$, $(J-K)_0$, and $(B-K)_0$ colors, and Mg2 index. We have chosen to present the various relations using the GC $(V-I)_0$ colors directly instead of transforming these to metallicities. It should be kept in mind that some of the low-luminosity galaxies contain rather few GCs, so that peaks in their $(V-I)_0$ color distributions may not be very well determined. The open dots in Fig. 12 indicate data for the Fornax galaxies (NGC 1399, NGC 1404) which were transformed from $B-I$ to $V-I$.

The dashed lines in each panel of Fig. 12 represent least-squares fits to the data points. Slopes and Spearman rank correlation tests for the various fits are listed in Table 10. The colors of *both* red and blue GCs are correlated with host galaxy M_B and central velocity dispersion ($\log \sigma_0$) with a $> 90\%$ probability, while trends with the Mg2 index and host galaxy colors are only weak and, in the case of Mg2, mostly driven by the poor GC system of NGC 4733. The correlations with host galaxy M_B and $\log \sigma_0$ are all significant at the $2-3\sigma$ level, and remain relatively unchanged even

if the two cluster-poorest galaxies, NGC 3384 and NGC 4733 are omitted from the fits. Although correlations for the blue and red GC populations are found at about the same significance level, the slope is generally slightly steeper for the red GC correlations.

A correlation between the color of the *red* GCs and host galaxy luminosity was already noticed by Forbes, Brodie and Grillmair (1997). These authors did not find any convincing correlation with the color of the *blue* peak but only a large scatter. Forbes, Brodie and Grillmair (1997) used a fairly heterogeneous dataset with metallicities derived from a mixture of spectroscopy, $V-I$, $B-I$ and Washington photometry, which might explain why they failed to detect any correlation between the metallicity of the metal-poor GC populations and host galaxy properties. Based on a larger (but still somewhat heterogeneous) sample, Burgarella, Kissler-Patig & Buat (2001) detected a correlation between host galaxy M_V and the metallicity of the blue peak. The slope of their [Fe/H] $- M_V$ fit (-0.06 ± 0.01) is formally quite similar to that of our $(V-I)_0 - M_B$ relation, assuming a conversion factor of about 3 between $(V-I)_0$ and [Fe/H] (Kissler-Patig et al. 1998). However, excluding the cluster-poorest galaxies from their sample, Burgarella, Kissler-Patig & Buat (2001) found that the slope of their [Fe/H] vs. M_V relation was reduced to -0.02 ± 0.02. They did not look at the red GCs.

Based on a compilation of literature data, Forbes & Forte (2000) detected a 3σ correlation between $\log \sigma_0$ and the color of the red peak. The slope of their relation (0.23) is quite similar to the one found here. Forbes & Forte (2000) found no significant correlation between $\log \sigma_0$ and the color of the blue peak, but their data comfortably allow a slope similar to the one indicated in our Fig. 12. Finally, we note that Kundu (1999) found the colors of both red and blue GCs to be at best weakly correlated with host galaxy luminosity.

One of the more remarkable features of Fig. 12 is the lack of any clear correlation between host galaxy *colors* and the GC colors. In *most* galaxies, the colors of the red GCs roughly match the $(V-I)_0$ color of the galaxy halo light, but galaxy colors span a wider range than the red GC populations and several galaxies have much redder integrated $(V-I)_0$ colors than the red GCs. As an illustration of this, we have superimposed a dashed-dotted line corresponding to a 1:1 correspondance between GC and host galaxy $V-I$ colors on Fig. 12. Such a relation is clearly incompatible with the data. At best, we see a weak correlation between the host galaxy $(J-K)_0$ color and the color of the *red* GC population, but a slope of 0 is within the $1.5\,\sigma$ errors even for this relation. Since it is well-known that a relation exists between the integrated color and the luminosity of early-type galaxies (e.g. van den Bergh 1975; Sandage & Visvanathan 1978), it is somewhat puzzling that we do not detect correlations between the GC colors and *both* host galaxy luminosity and color. In fact, a linear fit to the host galaxy $(V-I)_0$ and M_B values for the galaxies in our sample, listed in Table 2, yields $(V-I)_0 = (-0.046 \pm 0.007)\, M_B + 0.253$. If this is combined with the slopes of -0.016 ± 0.005 and -0.020 ± 0.008 for the GC color vs. host galaxy M_B fits (Table 10) then one would expect slopes of 0.35 ± 0.11 and 0.43 ± 0.17 for the GC color vs. host galaxy $(V-I)_0$ relations. For the blue peak this is actually compatible with the measured slope within the 1σ errors, while there is a $\sim 2\sigma$ discrepancy for the red peak. The main reason for

this is probably that the galaxy color–luminosity relations exhibit significant scatter. For example, inspection of Table 2 shows that NGC 4472 has very blue $(V-I)_0$ and $(J-K)_0$ colors for its high luminosity, while the much less luminous NGC 4473 has the *reddest* integrated $(V-I)_0$ colors of all the galaxies in the sample. Thus, globular cluster colors appear to be determined primarily by the host galaxy luminosity, rather than by whatever processes gave the field stars their colors.

6.2. GC subpopulations and formation scenarios

The presence of a correlation between GC colors and host galaxy luminosities for both red and blue GCs would be a strong indicator that both GCs populations "knew" about the galaxy in which they formed. However, the lack of any obvious correlation between host galaxy $V-I$ *color* and the GC colors potentially provides us with an equally strong clue that the cluster- and star formation histories of galaxies may have been significantly different. This should come as no surprise – as is well known, the Milky Way is still an actively star forming galaxy, while globular cluster formation ceased long ago in our Galaxy.

The discovery of bimodal color distributions in many galaxies has led various authors to speculate about formation scenarios that could create distinct GC subpopulations. As mentioned in the introduction, the merger model by Ashman and Zepf (1992) was the first to explicitly predict bimodal colors distributions. In this model, elliptical galaxies form by mergers of gas-rich spirals, creating the metal-rich GC population in the starburst associated with the merger. The metal-poor clusters are inherited from the progenitor galaxies. One major problem with this model, however, is the fact that spirals generally contain only few globular clusters, and that most large ellipticals are rich in both metal-rich and metal-poor GCs. Gas-rich mergers might account for relatively cluster-poor ellipticals, but the exceedingly rich GC systems of galaxies like NGC 4486 and NGC 4472 are very hard to explain within the merger picture (Harris 1999).

Alternatively, it has been suggested that the *metal-rich* GCs in ellipticals represent the galaxies' original GCs, while the metal-poor ones have been accreted from smaller galaxies (Côté, Marzke and West 1998) and/or formed in minor mergers. Their model is able to successfully account for quite a wide variety of final metallicity distributions. A somewhat similar approach was taken by Hilker et al. (1999) who suggested that the metal-poor GCs in ellipticals formed by accretion of gas-rich dwarfs. One remaining problem with this approach is to verify that it is actually possible to accrete the required larger numbers of GCs without accreting any appreciable number of metal-poor *field stars* at the same time.

It is, however, still not clear how to explain the wide range in observed properties of GC color distributions. Some galaxies exhibit strikingly bimodal color distributions with roughly equal numbers of blue and red GCs (like e.g. NGC 1404, NGC 4649, NGC 4472), while others show a much reduced number of red GCs (NGC 4406) or even just a single (but still significantly broadened) metal-poor component (NGC 4365), and still others appear to show a fairly continuous color

distribution, spanning a range similar to that observed in the truly bimodal systems (NGC 4552).

If mergers or accretion played an important role, one might expect a dependence on environment. In Fig. 13 we plot the two indicators of bimodality, P(kmm) and P(dip) as a function of galaxy density (Tully 1988). For P(kmm), a low value (close to 0) indicates that a two-component fit is a major improvement relative to a one-component fit. For P(dip), a high value (close to 1) indicates a high probability that the dataset is not unimodal. Although current galaxy density is a quite crude measure of past mergers, neither of the two plots shows any significant correlation with galaxy density, suggesting that the population mixture in GC systems is mostly shaped by intrinsic processes in the galaxies.

One possible signature of past mergers is kinematically distinct cores (KDCs). Among the galaxies in our sample, several have KDCs. However, the GC systems of these galaxies do not generally show strongly bimodal color distributions. In fact, one of these galaxies is NGC 4365 whose GC system appears to be composed almost entirely of a single metal-poor population. We also note that Forbes et al. (1996) found no evidence for any connection between KDCs in galaxies and bimodality.

Both mergers and accretion processes obviously take place even at the current epoch and it is clear that the starbursts associated with these events often lead to the formation of large numbers of very luminous (and therefore presumably massive) star clusters. However, the question is whether they were the dominating factors shaping the properties of GC systems in large ellipticals. It is now clear that massive star clusters can form under a wide variety of circumstances (Larsen & Richtler 2000) and the high levels of star formation in the gas-rich environments in proto-galaxies may quite naturally have led to formation of globular clusters. The observation that the colors of *both* GC populations appear to correlate with host galaxy properties would be hard to explain within the accretion / merger pictures and would fit better into *in situ*-type scenarios in which all GCs "knew" about the size of the final galaxy to which they would eventually belong. In order for this to be possible, the initial episodes of GC formation in giant ellipticals (gEs) must have taken place *after* they assembled into individual entities, although not necessarily having evolved into anything we would recognize as a gE today.

Such a scenario was outlined by Forbes, Brodie and Grillmair (1997), who further proposed that the initial episode of GC formation would be halted by the dispersion of gas by supernova explosions. A few Gyrs later, as the gas cools down and falls deeper into the potential well, star formation commences again, forming the second (metal-rich) generation of stars and GCs. A very similar scenario was favored by Harris, Harris & Poole (1999) and Harris & Harris (2000), based on deep HST observations of the red giant branch in the nearby giant elliptical NGC 5128. They found an extremely broad metallicity distribution function for field stars in this galaxy, extending from [Fe/H] ~ -2 to at least solar, which was remarkably well matched by a two-component model of simple closed-box chemical evolution.

One might argue that the distinction between the various formation scenarios is somewhat

blurred at the earliest epochs. Harris, Harris & Poole (1999) point out that the first generation of star formation within the halo of a proto-gE may well have proceeded within a large number of relatively distinct gaseous clumps. In a proto-galactic halo with numerous gaseous fragments, many of these fragments are bound to interact and form larger subunits. Such events would share many of the characteristics of "mergers", especially when two relatively large subunits collide. In some occasions, such large-scale events could lead to a major burst of GC formation in which much of the remaining gas would be consumed, forming a quite distinct second peak in the metallicity distribution as observed in e.g. NGC 4649.

Even if some characteristics of GC systems might be understood within a framework like the one outlined above, many observed properties evidently remain to be accounted for. One remaining issue is to explain the *size* difference between GC subpopulations. This phenomenon seems to be a quite ubiquitous one, observed in all galaxies with broad GC color distributions (even in the Milky Way!) and at all galactocentric distances. The size differences may be either primordial, or a result of dynamical evolution. The fact that the differences exist in all galaxies and at all radii would appear to indicate a high probability that the differences are actually set up at formation. Since more compact clusters presumably originated from denser proto-globular gas clouds, this may hold information about the physical condition of the gas phase and star formation processes at the time of GC formation. The physics of cluster formation is still very poorly understood, but observations of young globular-like clusters in nearby galaxies may very well hold important clues to a better understanding of this important issue. Another challenge is to understand the lack of any significant correlation between host galaxy colors and GC colors. One could speculate that globular clusters form preferentially during the first, burst-like phases of major star forming episodes, while field stars continue to form in residual, enriched gas which was not used up initially in much the same way as stars are forming in the Milky Way today. However, a better understanding of star forming processes, particularly in the early Universe, is necessary before such ideas can be put on firmer ground.

7. Summary and conclusions

Using deep HST / WFPC2 data, we have performed a detailed analysis of the color, size and luminosity distributions of globular clusters in 17 nearby galaxies. The main results may be summarized as follows:

- In all but a few cases, a KMM test finds that two Gaussians provide a significantly improved fit to the color distribution relative to a single Gaussian. Simple histograms of the color distributions or a DIP test do not always confirm significant bimodality even in cases where the KMM test returns a very high confidence level for a two-component fit, but the peaks in the $(V-I)_0$ color distributions found by KMM are nevertheless quite consistent even in the less obviously bimodal cases.

- Red GCs are generally smaller than blue GCs by typically $\sim 20\%$. This is true also in galaxies without sharply defined bimodal color distributions and within "sub-bins" in color. In all galaxies, GC sizes decrease as a function of $(V-I)_0$ color in the range $0.70 < (V-I)_0 < 1.20$, while the sizes of the very reddest clusters ($(V-I)_0 > 1.20$) are again larger in some galaxies. When subdividing the clusters into only two broad bins, this effect can sometimes conceal a size difference between red and blue GCs.

  The GC size difference exists not only in ellipticals and S0 galaxies, but also in the one Sa galaxy (M104) in our sample. Perhaps even more remarkably, GCs in the *Milky Way* follow the exact same trend.

- Fitting t_5 functions to the globular cluster luminosity functions, we find that the turn-over of the blue GCs is generally brighter than that of the red ones by about 0.4 mag on the average for the full sample. This difference is slightly larger than that expected from population synthesis models if the two populations have identical mass functions, ages and stellar IMFs, but different metallicities. However, if the sample is restricted to galaxies for which the error on the turn-over difference is less than 0.25 mag, then the average difference between the turn-overs of blue and red GCs is only 0.3 mag, which is very close to the 0.26 mag expected for similar ages and mass functions but different metallicities. The Milky Way and Sombrero spiral galaxies both show a similar offset of ~ 0.5 mag, but curiously, in M31 the *blue* (metal-poor) GCs seem to be fainter.

  Using luminosity instead of magnitude units, the upper part of the GCLF ($L \gtrsim 10^5 \mathrm{L}_\odot$) is generally well fit by a power-law with exponent $\alpha \sim -1.75$. Thus, the mass function of old GCs brighter than the turn-over is apparently very similar to that of young cluster systems, and it seems plausible that old GCs and young clusters form by the same basic mechanism.

- We have apparently detected a second case of "faint extended" clusters in the nearby S0-type galaxy NGC 3384, similar to those in NGC 1023 (Larsen and Brodie 2000). In the four galaxies in our sample where such objects are definitively detectable, they thus appear to exist in two. These extended clusters are generally fainter than the GCLF turn-over and thus tend to raise the lower end of the GCLF, making it deviate from the Milky Way GCLF. However, most of the galaxies in our sample are too distant to tell from current data if they possess similar clusters, so it remains unknown how common such objects are.

- In three cluster-rich galaxies with several pointings (NGC 4472, NGC 4486, NGC 4365) we have examined radial trends in GC size and color. The size difference in NGC 4472 and NGC 4486 between blue and red GCs exists at all radii and we find no evidence for any correlation between either the $(V-I)_0$ peak colors or GC sizes and distance from the galaxy centers in these two galaxies. NGC 4486 shows a strong increase in the relative numbers of blue and red clusters outwards. Within the HST fields, such a trend is much weaker in NGC 4472. NGC 4365 seems to host only one (metal-poor) GC population with no strong color gradients, but GCs in the outermost bins do tend to be larger in this galaxy.

- We have investigated correlations between the colors of GC subpopulations and host galaxy properties. Both the blue and red peak $(V-I)_0$ colors correlate at the $2-3\sigma$ level with host galaxy luminosity and central velocity dispersion. However, there is no evident correlation between GC colors and the colors of their host galaxies. Likewise, indicators of bimodality (KMM and DIP tests) show no correlation with surrounding galaxy density.

We conclude that our data are best explained within *in-situ* formation scenarios in which both GC populations formed within the potential well of the proto-galaxy, possibly in multiple episodes of star formation.

This work was supported by HST grants GO.05920.01-94A and GO.06554.01-95A, National Science Foundation grant number AST9900732, NATO grant CRG 971552 and Faculty Research funds from the University of California, Santa Cruz. We thank Markus Kissler-Patig for useful discussions and Ken Freeman for his help, and the helpful comments of an anonymous referee are appreciated.

REFERENCES

Abraham, R. G. & van den Bergh, S. 1995, ApJ, 438, 218

Ashman, K. M., Bird, C. M., and Zepf, S. E. 1994, AJ, 108, 2348

Ashman, K. M., Conti, A., and Zepf, S. E. 1995, AJ, 110, 1164

Ashman, K. M., and Zepf, S. E. 1992, ApJ, 384, 50

Ashman, K. M., Zepf, S. E. 1998, Globular Cluster Systems, Cambridge University Press

Barmby, P., Huchra, J. P., Brodie, J. P., Forbes, D. A., Schroder, L. L. & Grillmair, C. J. 2000, AJ, 119, 727

Barmby, P., Huchra, J. P., Brodie, J. P., 2001, AJ, in press (astro-ph/0011522)

Baum, W. A. 1955, PASP, 67, 328

Baum, W. A. et al. 1995, AJ, 110, 2537

Beasley, M. A., Sharples, R. M., Bridges, T. J., Hanes, D. A., Zepf, S. E., Ashman, K. M. & Geisler, D. 2000, MNRAS, 318, 1249

Bender, R. 1988, A&A, 202, L5

Bridges, T. J., Hanes, D.A., Harris, W.E. 1991, AJ, 101, 469

Bridges, T. J. et al. 1997, MNRAS, 284, 376

Brodie, J. P. & Huchra, J. P. 1991, ApJ, 379, 157

Burgarella, D., Kissler-Patig, M., Buat, V. 2001, AJ, in press (astro-ph/0101345)

Ciardullo, R., Jacoby, G. H., and Harris, W.E. 1991, ApJ, 383, 487

Cohen, J., Blakeslee, J., Ryzhov, A., 1998, ApJ, 496, 808

Côté, P., Marzke, R. O., and West, M. J. 1998, ApJ, 501, 554

Davies, R. L., Birkinshaw, M. 1988, ApJS, 68, 409

Dolphin, A. E. 2000, PASP, 112, 1397

Elmegreen, B. G. and Efremov, Y. N., 1997, ApJ, 480, 235

Elson, R. A. W., & Fall S. M. 1985, PASP, 97, 692

Elson, R. A. W. & Santiago, B. X. 1996, MNRAS, 278, 617

Elson, R. A. W. 1997, MNRAS, 286, 771

Forbes, D. A., Brodie, J. P., and Grillmair, C. J. 1997, AJ, 113, 1652

Forbes, D. A., and Forte, J. C. 2000, MNRAS, accepted, astro-ph/0005481

Forbes, D. A., Franx, M. J., Illingworth, G. D., Carollo, C. M. 1996, ApJ, 467, 126

Forbes D. A., Grillmair C. J., Smith R. C., 1997, AJ, 113, 1648

Forbes, D. A., Grillmair, C. J., Williger, G. M., Elson, R. A. W., Brodie, J. P. 1998, MNRAS, 293, 325

Ford, H. C., Hui, X., Ciardullo, R., Jacoby, G. H., Freeman, K. C., 1996, ApJ, 458, 455

Gebhardt, K. and Kissler-Patig, M. 1999, AJ, 118, 1526

Geisler, D., Lee, M. G. & Kim, E. 1996, AJ, 111, 1529

Golev, V., & Prugniel P. 1998, A&AS, 132, 255

Grillmair, C. J., Freeman, K. C., Bicknell, G. V., et al. 1994, ApJ, 422, 9

Grillmair, C. J., Forbes, D. A., Brodie, J. P., Elson, R. A. W. 1999, AJ, 117, 167

Harris, G. L. H., Harris, W. E. and Poole, G. B. 1999, AJ, 117, 855

Harris, G. L. H., Harris, W. E. 2000, AJ, 120, 2423

Harris, W. E., Harris, H. C., Harris G. L. H. 1984, AJ, 89, 216

Harris, W. E. and Pudritz, R. E. 1994, ApJ, 429, 177

Harris, W. E. 1991, ARA&A, 29, 543

Harris, W. E. 1996, AJ, 112, 1487

Harris, W. E. 1999, in: "Globular Clusters", Cambridge Contemporary Astrophysics, eds. C. M. Rogers, I. Pérez Fournón and F. Sánches, Cambridge University Press

Harris, W. E., Harris, G. L. H. & McLaughlin, D. E. 1998, AJ, 115, 1801

Harris, W. E. and van den Bergh, S. 1981, AJ, 86, 1627

Hartigan, J. A. & Hartigan, P. M. 1985, Ann. Stat., 13, 70

Hilker, M., Infante, L., and Richtler, T. 1999, A&AS, 138, 55

Holtzman, J. A., Burrows, C. J., Casertano, S., et al. 1995, PASP, 107, 1065

Holtzman, J. A., Watson, A. M., Mould, J. R., et al. 1996, AJ, 112, 416

Huchra, J. P. 1985, ESO Workshop on the Virgo Cluster, 181

Huchra, J. & Brodie, J. 1987, AJ, 93, 779

Jarrett, T. H., Chester, T., Cutri, R., Schneider, S., Skrutskie, M. & Huchra, J. P. 2000, AJ, 119, 2498

Johnson, K. E., Vanna, W. D., Leitherer, C., et al. 1999, AJ, 117, 1708

Johnson, K. E., Leitherer, C., Vacca, W. D., Conti, P. S. 2000, AJ, 120, 1273

Kent, S. M. 1988, AJ, 96, 514

King, I. R. 1962, AJ, 67, 471

Kissler, M., Richtler, T., Held, E. V. et al. 1994, A&A, 287, 463

Kissler-Patig, M., Richtler, T., Hilker, M., 1996, A&A, 308, 704

Kissler-Patig, M., Richtler, T., Storm, J., della Valle, M., 1997, A&A, 327, 503

Kissler-Patig, M., Brodie, J. P., Schroder, L. et al., 1998, AJ, 115, 105

Krist, J., and Hook, R. 1997, "The Tiny Tim User's Guide", STScI

Kundu, A., and Whitmore, B. C. 1998, AJ, 116, 2841

Kundu, A. 1999, PhD thesis, Univ. of Maryland

Kundu, A., Whitmore, B. C., Sparks, W. B., et al. 1999, ApJ, 513, 733

Larsen, S. S. 1999, A&AS, 139, 393

Larsen, S. S., and Brodie, J. P., 2000, AJ, 120, 2938

Larsen, S. S., Forbes, D. A., & Brodie, J. P., 2001, MNRAS, submitted

Larsen, S. S., & Richtler T., 2000, A&A 354, 836

Lee, M. G., & Geisler, D. 1993, AJ, 106, 493

Lee, M. G., Kim, E., Geisler, D., 1998, AJ, 115, 947

Lee, M. G., Kim, E., 2000, AJ, 120, 260, astro-ph/0004116

McLaughlin, D. E., Secker, J., Harris, W. E. & Geisler, D. 1995, AJ, 109, 1033

McMillan, R., Ciardullo, R., Jacoby, G. H. 1993, ApJ, 416, 62

Mould, J. R., Oke, J. B. & Nemec, J. M. 1987, AJ, 93, 53

Neilsen, E. H., Jr. & Tsvetanov, Z. I. 2000, ApJ, 536, 255

Prugniel, P., & Heraudeau P. 1998, A&AS, 128, 299

Puzia, T. H., Kissler-Patig, M., Brodie, J. P., and Huchra, J. P. 1999, AJ, 118, 2734

Rangarajan, F.V.N, et al. 1995, MNRAS, 277, 1047

Rhode, K. L., & Zepf, S. E. 2001, AJ, 121, 210

Sakai, S., Madore, B. F., Freedman, W. L. et al. 1997, ApJ, 478, 49

Sandage, A. & Visvanathan, N. 1978, ApJ, 223, 707

Schlegel, D. J., Finkbeiner, D. P., and Davis, M. 1998, ApJ, 500, 525

Secker, J. 1992, AJ, 104, 1472

Simard, L. & Pritchet, C. J. 1994, AJ, 107, 503

Simien, F., Prugniel, P., 1997, A&AS, 126, 15

Stetson, P. B. 1998, PASP, 110, 1448

Strom, S. E., Strom, K. M., Wells, D. C. et al. 1981, ApJ, 245, 416

Tully, B. 1980, ApJ, 237, 390

Tully, B. 1988, Nearby Galaxies Catalog, Cambridge University Press

van den Bergh, S. 1975, ARA&A, 13, 217

van den Bergh, S., Lafontaine, A. 1984, AJ, 89, 1822

van den Bergh, S., 1983, PASP, 94, 640

van den Bergh, S., 1996, AJ, 112, 2634

Whitmore, B. C., Zhang, Q., Leitherer, C. et al. 1999, AJ, 118, 1551

Williams, R. M., Blacker, B., Dickinson, M. et al. 1996, AJ, 112, 1335

Zepf, S. E., Ashman, K. M., English, J. et al. 1999, AJ, 118, 752

Zepf, S. E., Beasley, M. A., Bridges, T. J., Hanes, D. A., Sharples, R. M., Ashman, K. M. & Geisler, D. 2000, AJ, 120, 2928

Zhang, Q. & Fall, S. M. 1999, ApJ, 527, L81

Zinn, R., 1985, ApJ, 293, 424

This preprint was prepared with the AAS LaTeX macros v5.0.

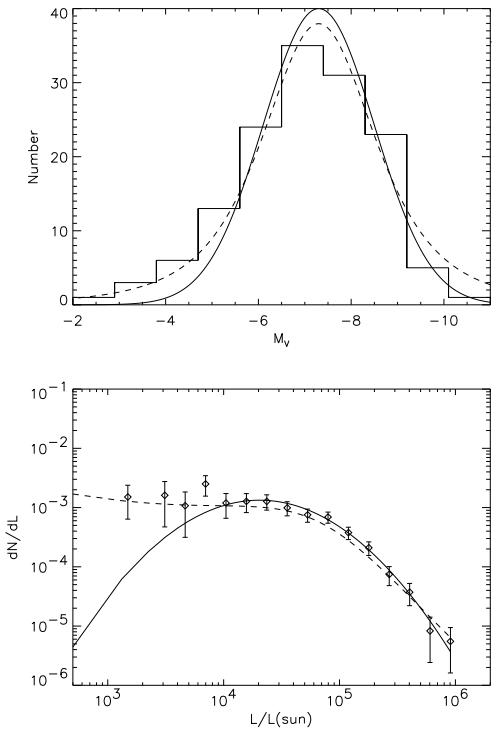

Fig. 1.— Luminosity function in magnitude units (left) and luminosity units (right) for globular clusters in the Milky Way. Overplotted are Gaussian (solid line) and t_5 function (dashed line) fits.

NGC 524

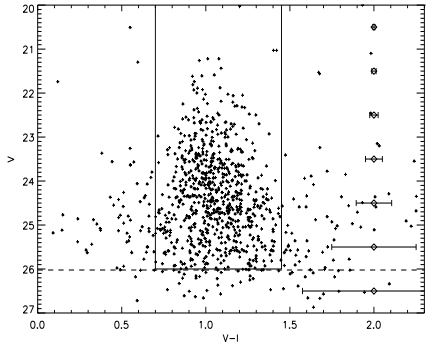

NGC 1023

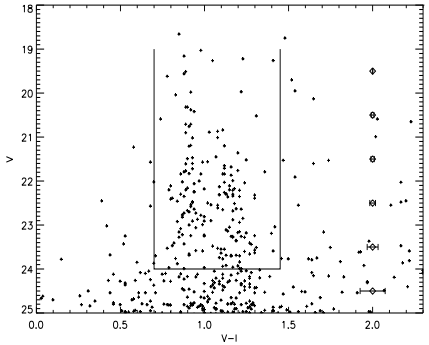

NGC 3115

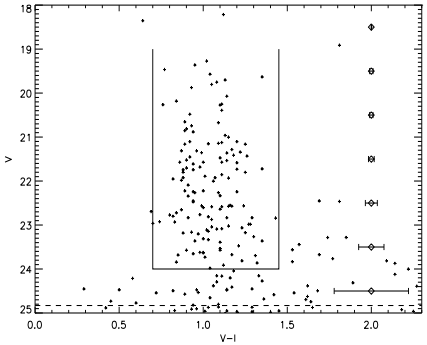

NGC 3379

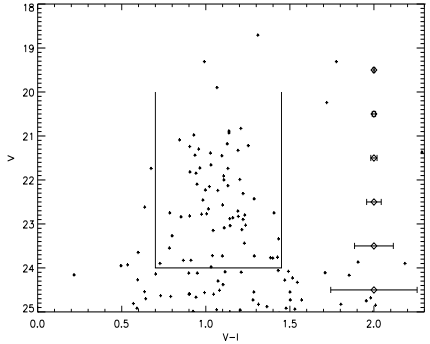

NGC 3384

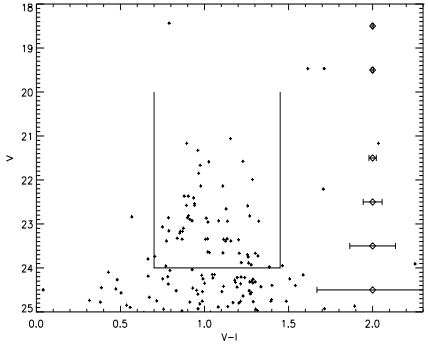

NGC 4365

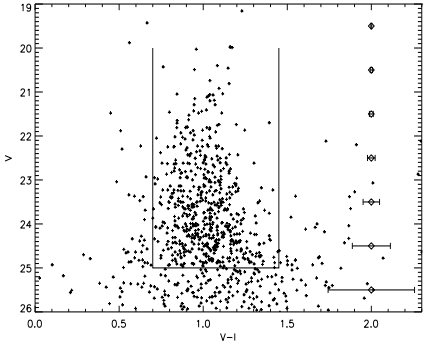

NGC 4406

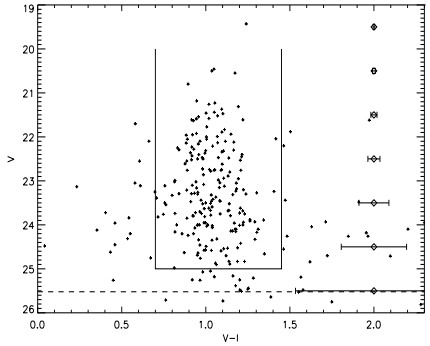

NGC 4472

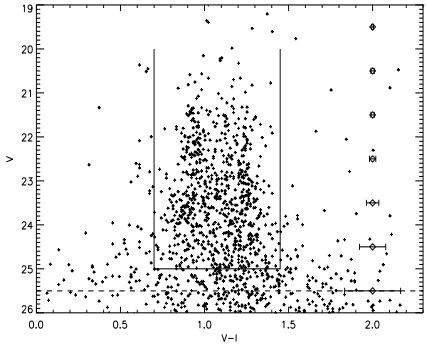

NGC 4473

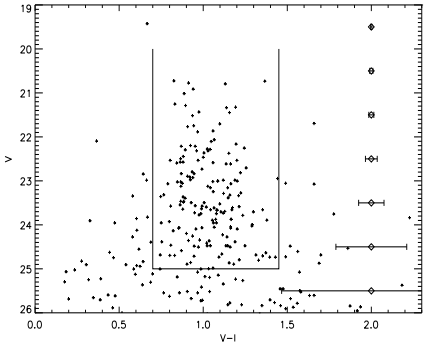

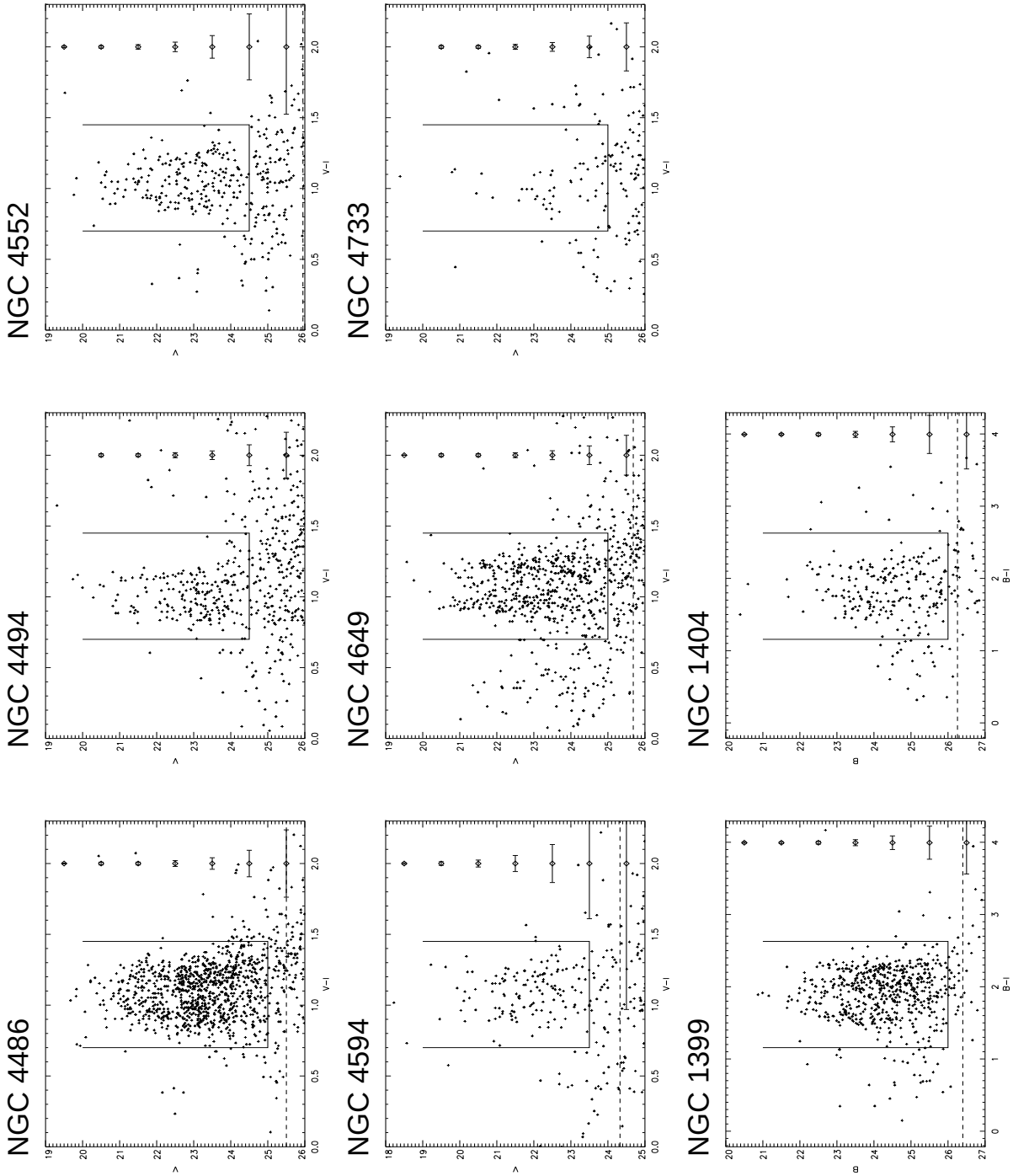

Fig. 2.— $(V-I)_0, V$ color-magnitude diagrams for the galaxies. The boxes indicate the part of the CMDs within which globular cluster candidates were selected and the horizontal dashed lines indicate approximate 50% completeness limits.

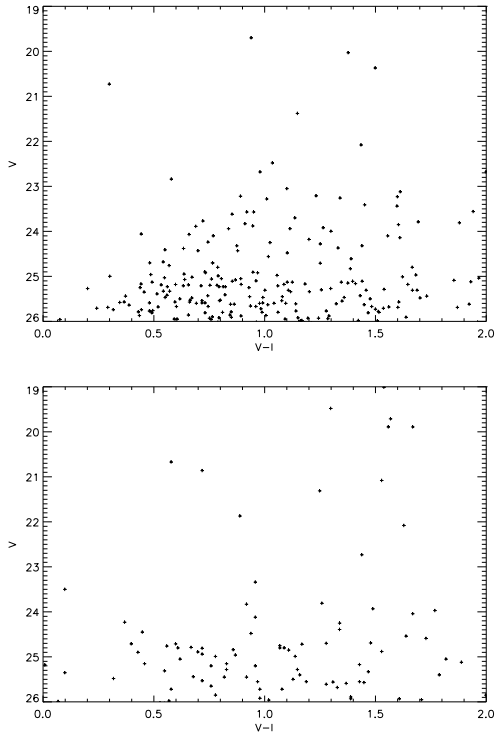

Fig. 3.— $(V-I)_0, V$ color-magnitude diagrams for the two comparison fields. Left: the Hubble Deep Field (North). Right: A field located about 2 deg from NGC 1023.

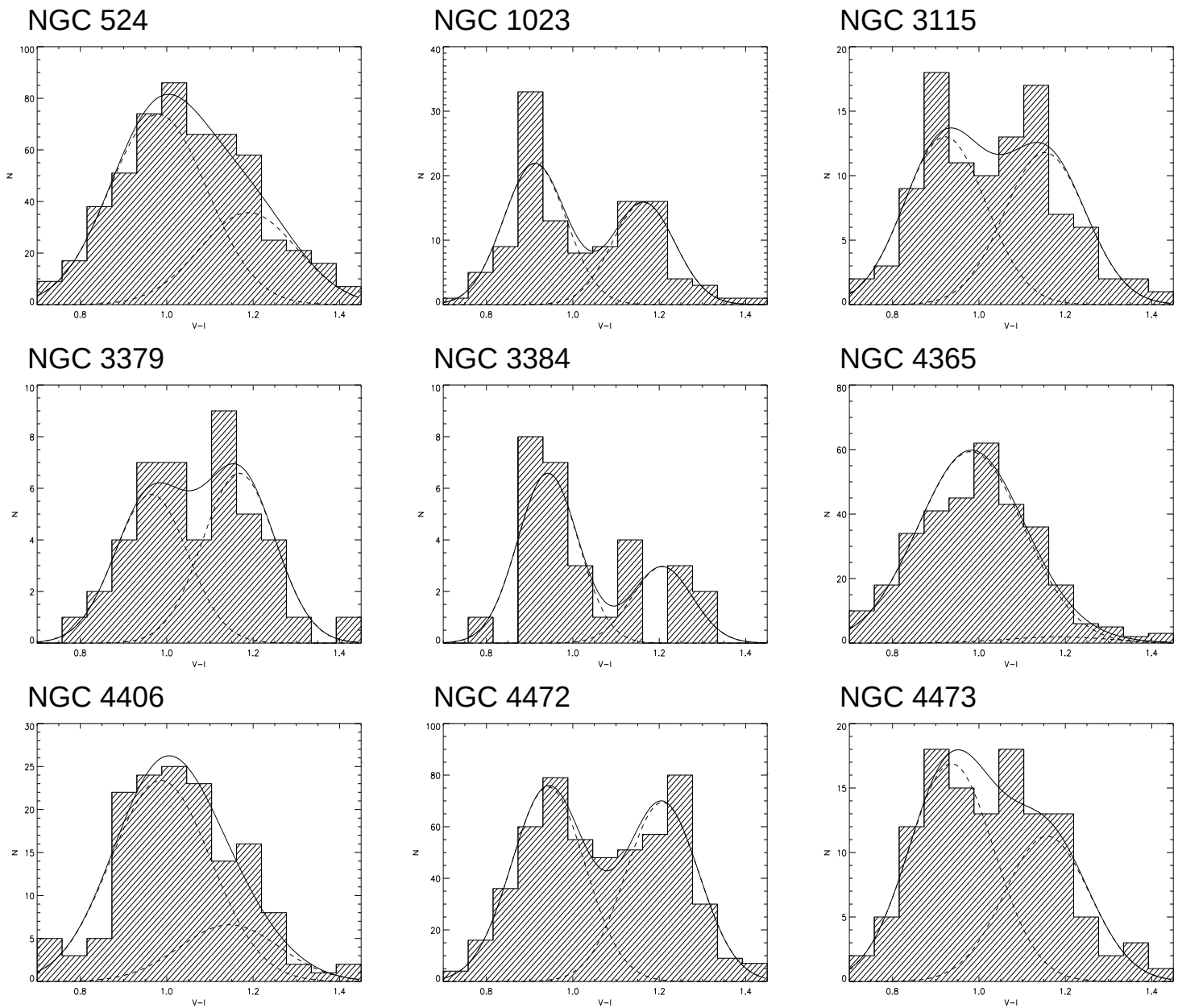
NGC 524
NGC 1023
NGC 3115
NGC 3379
NGC 3384
NGC 4365
NGC 4406
NGC 4472
NGC 4473
N
V−I

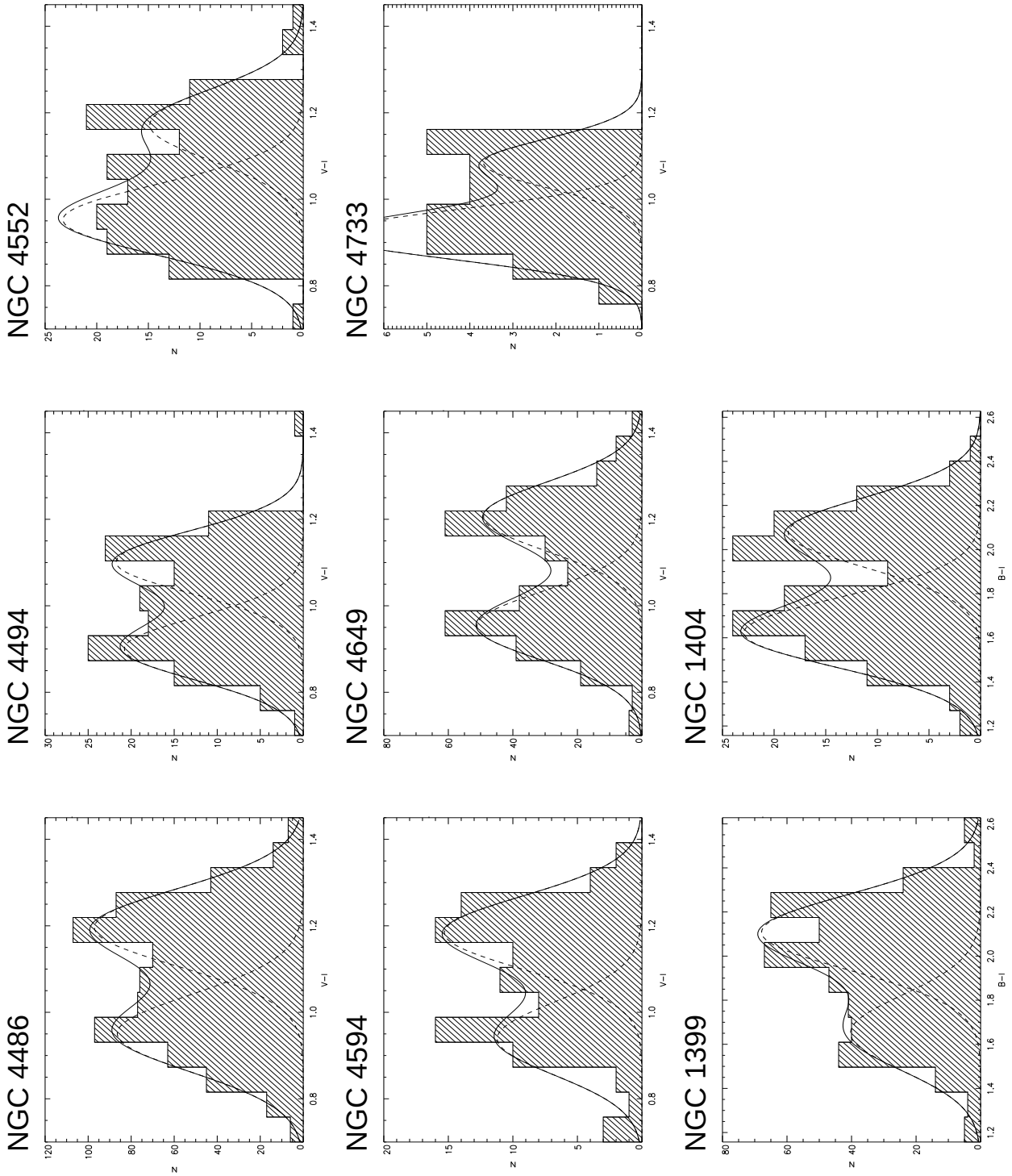

Fig. 4.— Histograms for the $(V-I)_0$ color distributions of GCs. Overplotted on the histograms are Gaussians corresponding to the two color peaks found by the KMM test and their sum.

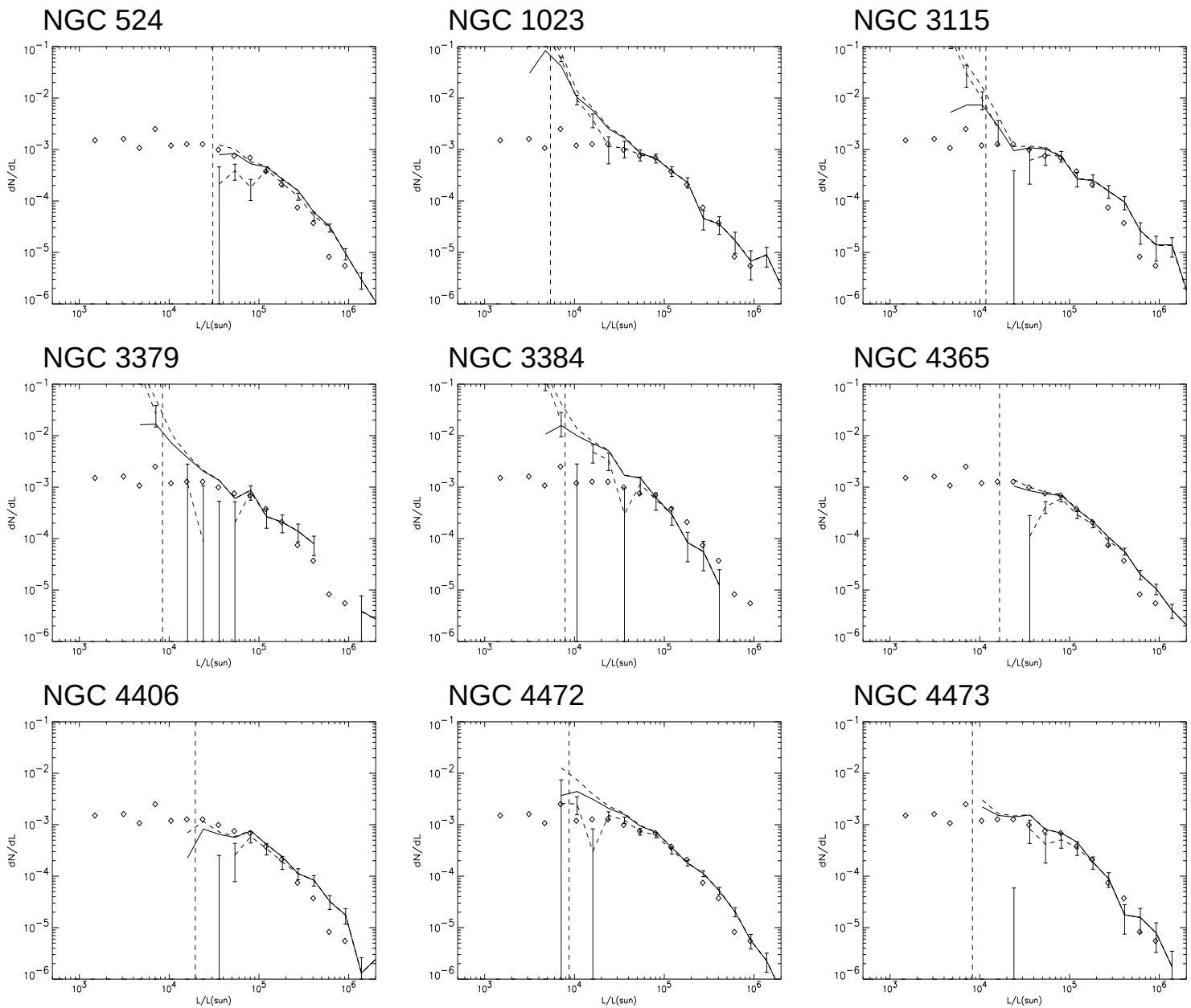
NGC 524
NGC 1023
NGC 3115
NGC 3379
NGC 3384
NGC 4365
NGC 4406
NGC 4472
NGC 4473
dN/dL
L/L(sun)

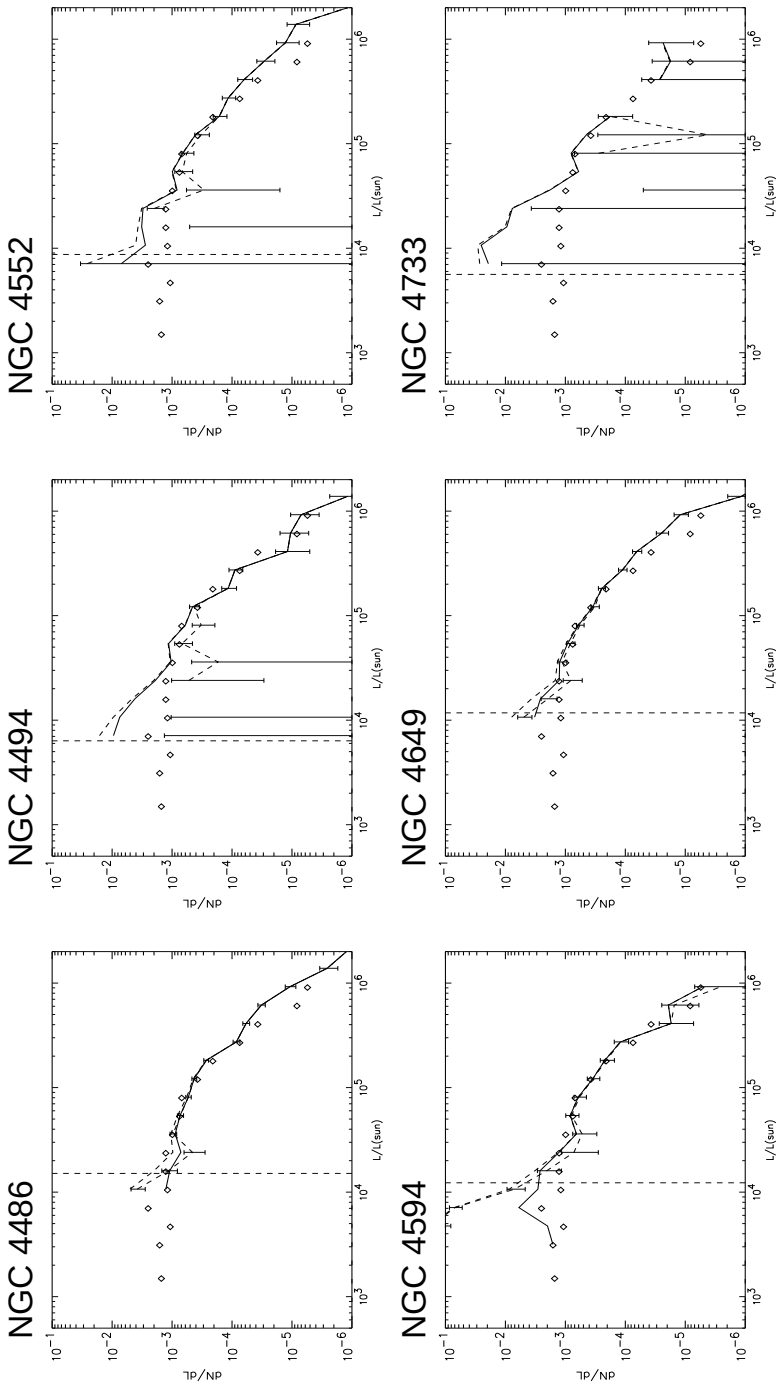

Fig. 5.— Luminosity functions for globular clusters in the 15 galaxies with V, I photometry, compared with the Milky Way GCLF (dots). The various lines in each plot represent the same data, but different assumptions about completeness / contamination corrections (see text for details). The turn-over magnitude of $M_V = -7.5$ corresponds to about $8 \times 10^4 \mathrm{L}_\odot$.

NGC 524

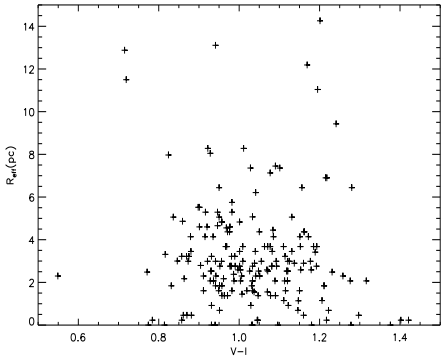

NGC 1023

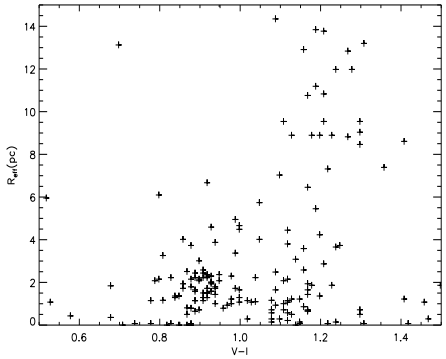

NGC 3115

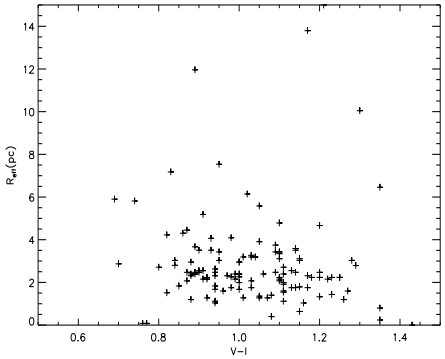

NGC 3379

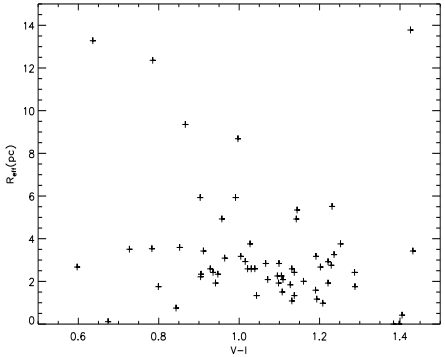

NGC 3384

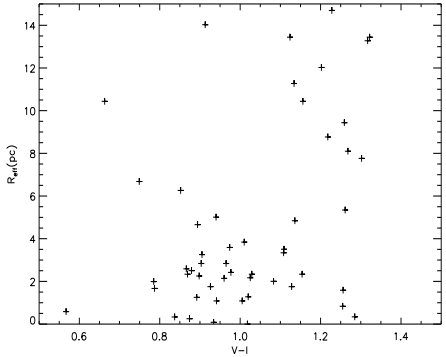

NGC 4365

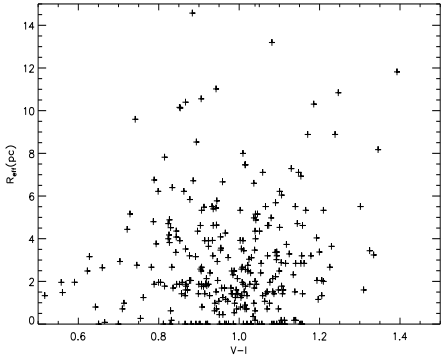

NGC 4406

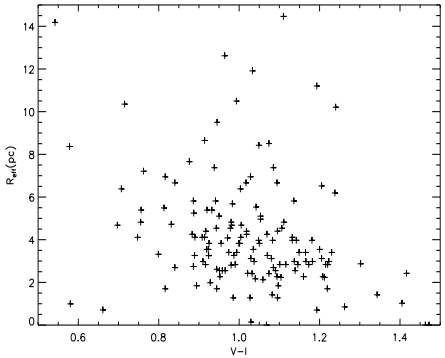

NGC 4472

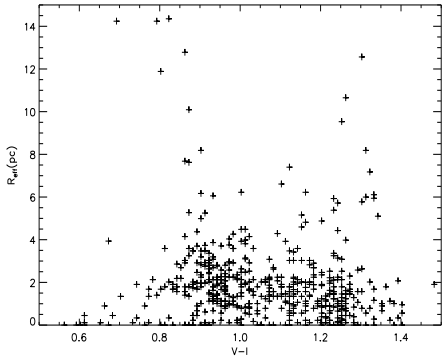

NGC 4473

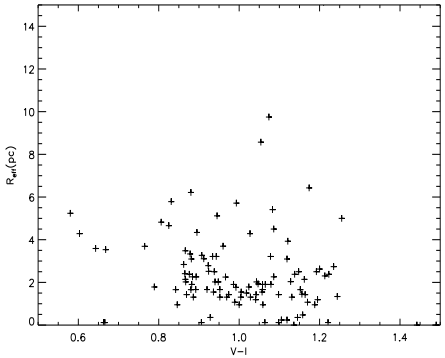

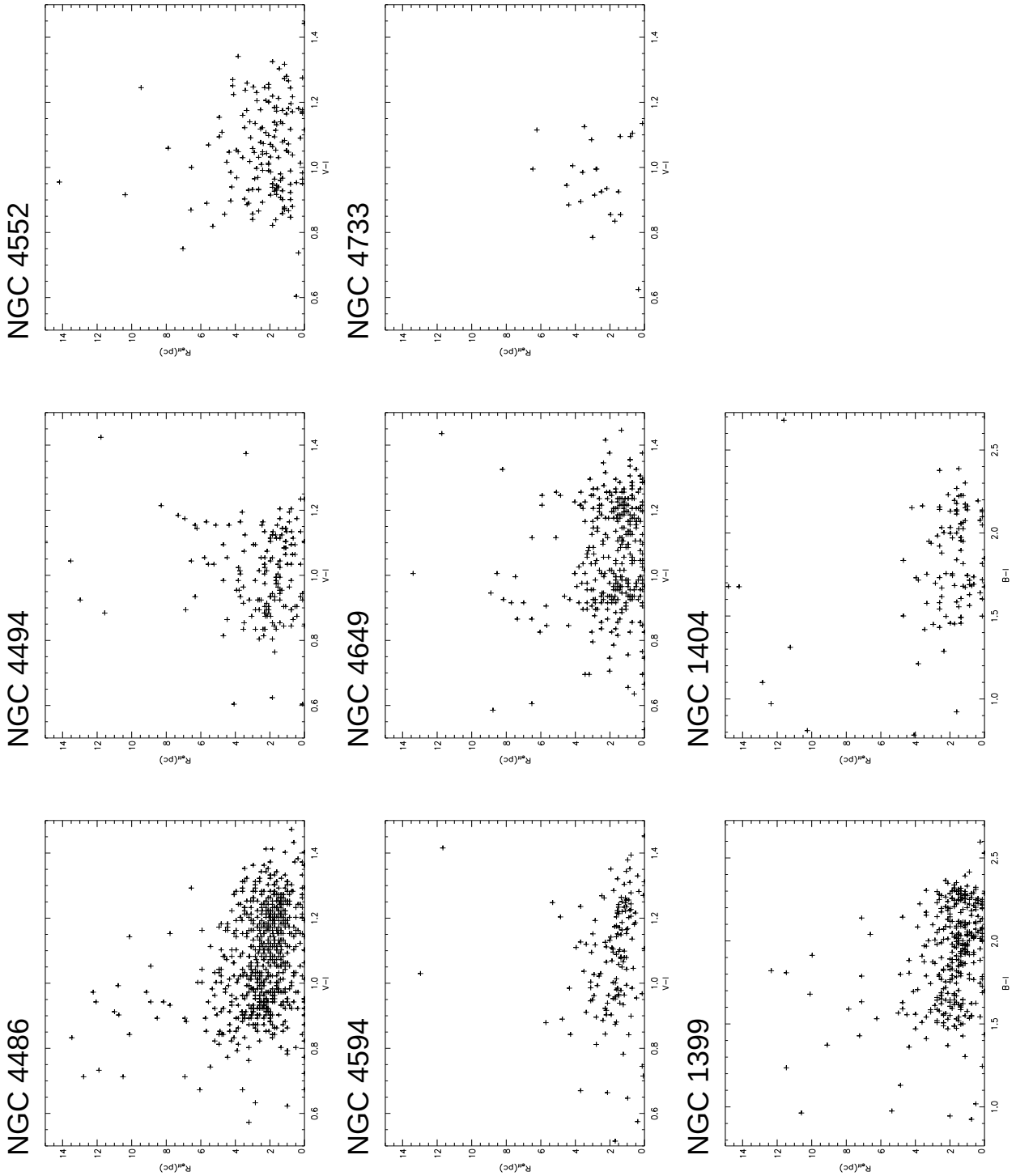

Fig. 6.— Size as a function of color for globular clusters in the galaxies.

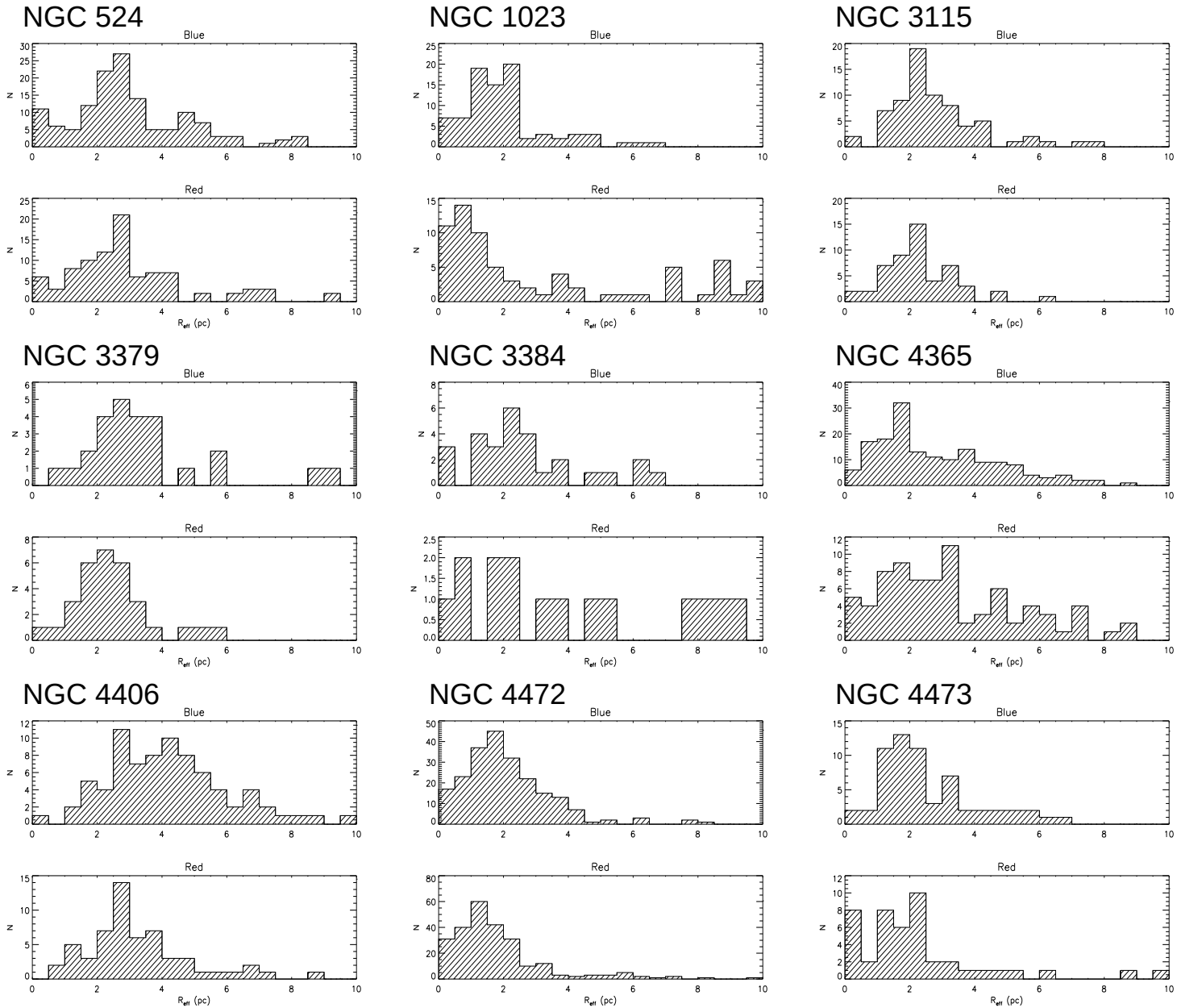
NGC 524
NGC 1023
NGC 3115
NGC 3379
NGC 3384
NGC 4365
NGC 4406
NGC 4472
NGC 4473
Blue
Red
N
R_{eff} (pc)

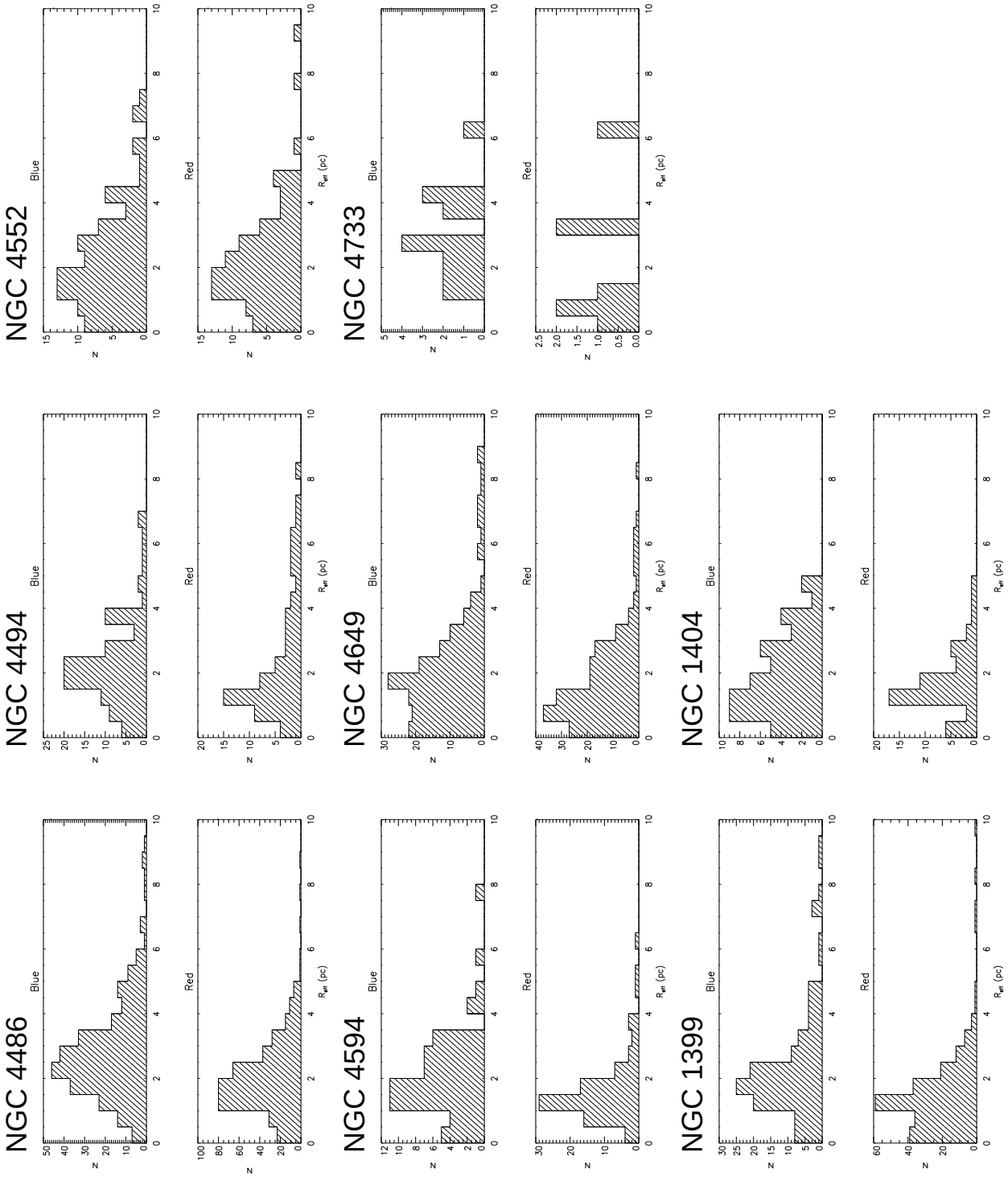

Fig. 7.— Size distributions for blue ($(V-I)_0 < 1.05$) and red ($(V-I)_0 > 1.05$) globular clusters. In each panel, the upper plot is for blue GCs and the lower plot is for red GCs.

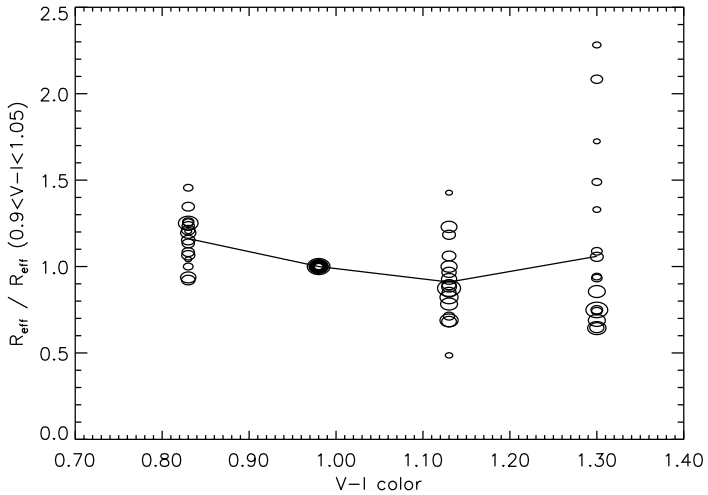

Fig. 8.— Comparison of GC sizes in four $(V-I)_0$ bins. Sizes have been normalized to 1.0 in the $0.90 < (V-I)_0 < 1.05$ bin. The symbol sizes are proportional to the logarithm of the number of GCs corresponding to each datapoint. The line indicates the (unweighted) average of all data points at each bin.

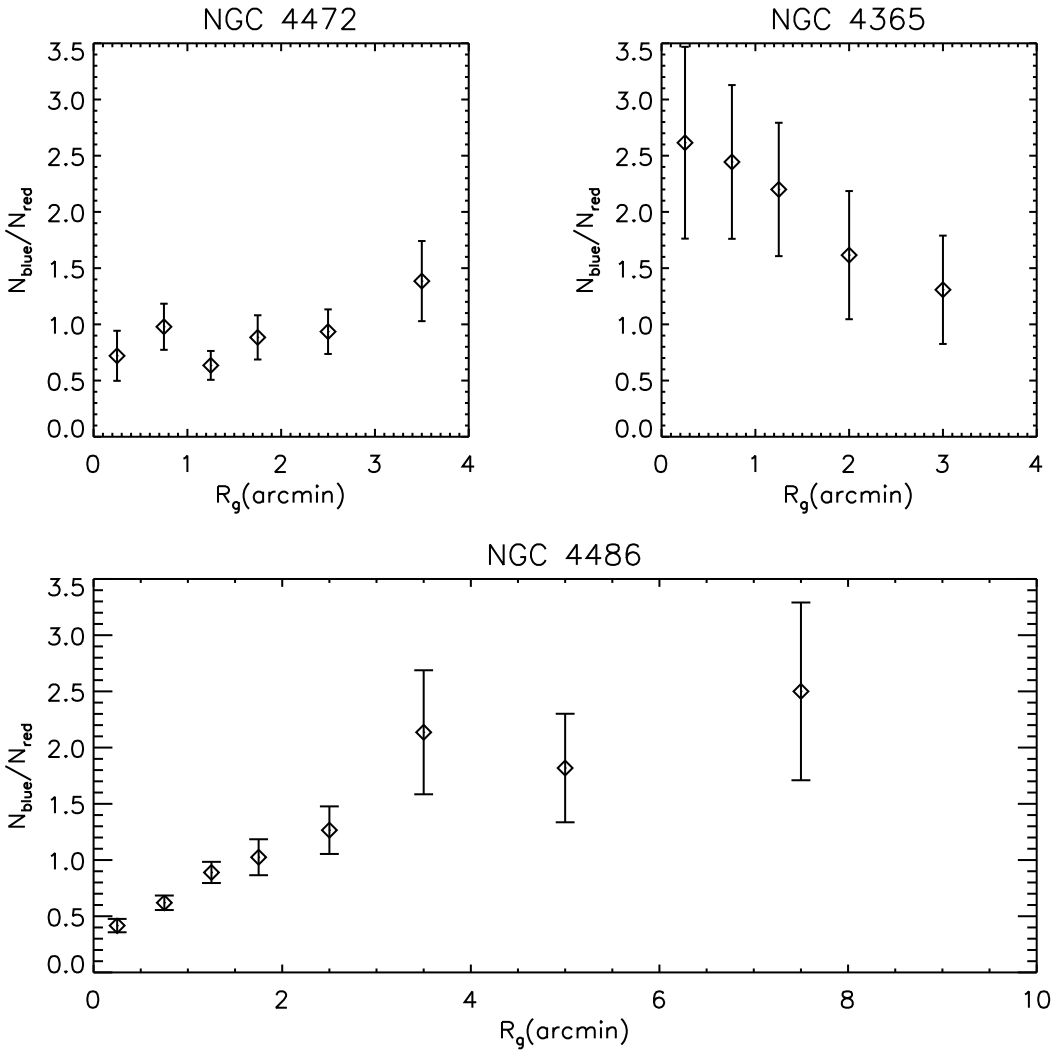

Fig. 9.— Ratio of the numbers of blue and red clusters as a function of galactocentric distance in arcmin (R_g) for NGC 4365, NGC 4472 (M49) and NGC 4486 (M87). At the distance of these galaxies, one arcmin equals about 4.6 kpc.

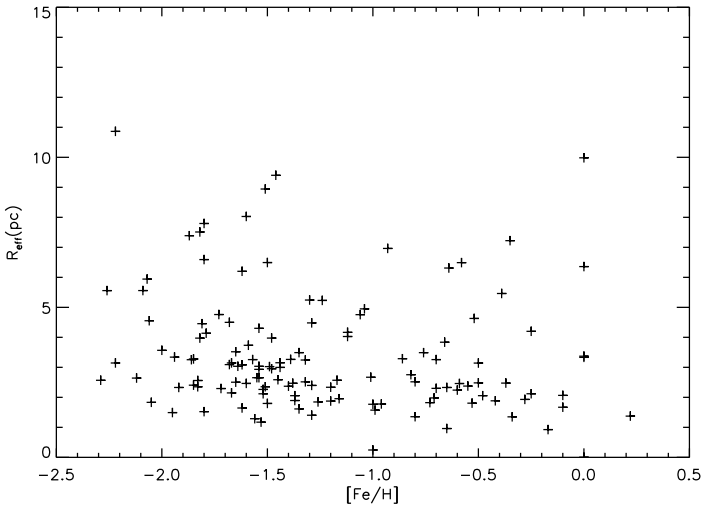

Fig. 10.— Effective radii for Milky Way GCs as a function of metallicity.

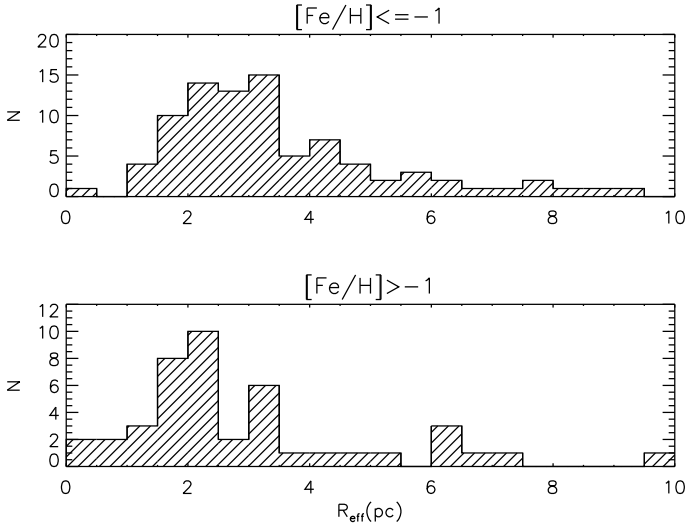

Fig. 11.— Size distribution for metal-poor ([Fe/H] < -1) and metal-rich ([Fe/H] > -1) globular clusters in the Milky Way.

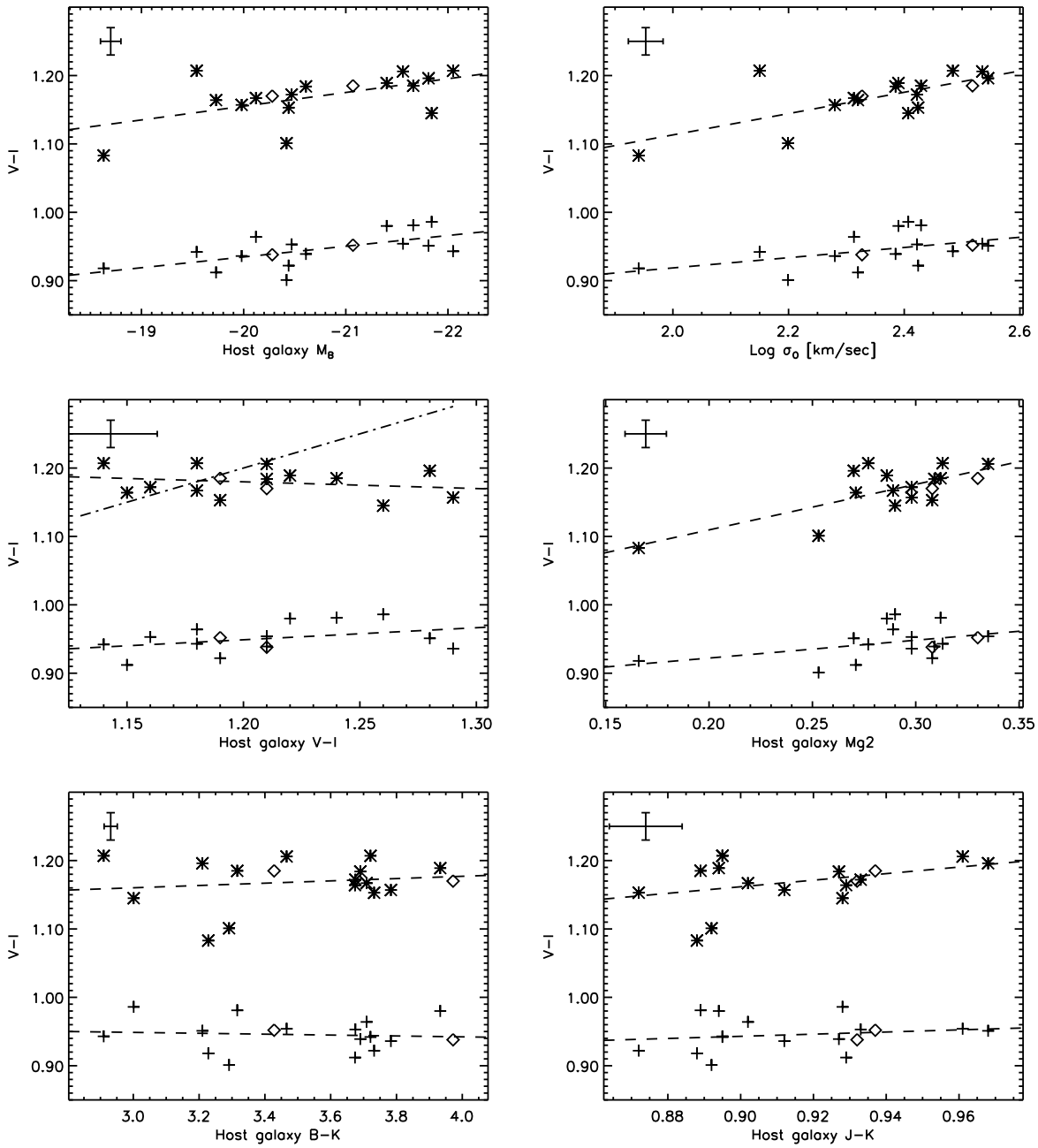

Fig. 12.— $(V-I)_0$ colors of the two peaks in the GC color distributions found by the KMM test as a function of host galaxy B magnitude, central velocity dispersion, host galaxy $(V-I)_0$, $(B-K)_0$ and $(J-K)_0$ color and Mg2 index. Asterisks ($*$) indicate the red peak, plus (+) markers the blue. Open diamonds indicate data for NGC 1399 and NGC 1404, transformed from $B-I$. The dashed lines are least-squares fits to the data. The dashed-dotted line in the host galaxy $(V-I)_0$ plot corresponds to a 1:1 relation between host galaxy and GC colors.

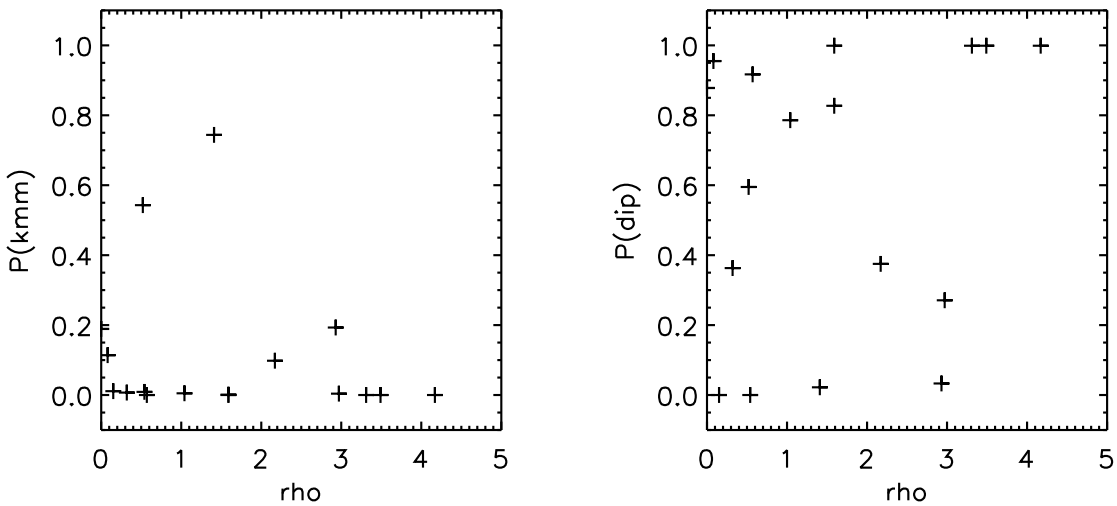

Fig. 13.— Indicators of bimodality as a function of galaxy density. For P(kmm), a value close to 0 indicates that two Gaussian functions are a significant improvement relative to only one when fitting the color distribution. For P(dip), a value close to 1 indicates a high probability that the color distribution is not unimodal.

Table 1: Data for observations of galaxies discussed in this paper. Suffix '-O' indicates exposures which are offset from the galaxy center. [a]F450W. [b]F547M.

Galaxy	PI / PID	T_{exp} (sec)	
		F555W	F814W
NGC 524	Brodie / 6554	2300	2300
NGC 524-O	Brodie / 6554	2400	2300
NGC 1023	Brodie / 6554	2400	2400
NGC 1023-O	Brodie / 6554	2400	2400
NGC 1399	Grillmair / 5990	2600[a]	1200
NGC 1404	Grillmair / 5990	2600[a]	1600
NGC 3115	Faber / 5512	1050	1050
NGC 3379	Faber / 5512	1660	1200
NGC 3384	Faber / 5512	1050	1050
NGC 4365	Brodie / 5920	2200	2300
NGC 4365-O	Brodie / 6554	2200	2200
NGC 4406	Faber / 5512	1500	1500
NGC 4472	Westphal / 5236	1800	1800
NGC 4472-O1	Brodie / 5920	2200	2300
NGC 4472-O2	Brodie / 5920	2200	2300
NGC 4473	Faber / 6099	1800	2000
NGC 4486	Macchetto / 5477	2400	2400
NGC 4486-O1	Macchetto / 6844	2000	2000
NGC 4486-O2	Macchetto / 6844	2000	2000
NGC 4486-O3	Biretta / 7274	2200	2500
NGC 4486-O4	Macchetto / 6844	1000	1000
NGC 4494	Brodie / 6554	2400	1800
NGC 4494-O	Brodie / 6554	2400	1600
NGC 4552	Faber / 6099	2400	1500
NGC 4594	Faber / 5512	1200[b]	1050
NGC 4649	Westphal / 6286	2100	2500
NGC 4733	Brodie / 6554	2200	2200

Table 2. Host galaxy properties

Galaxy	Type	$m-M$	M_B	A_B	$\log\sigma_0$ [km/sec]	$(V-I)_0$	$(B-K)_0$	$(J-K)_0$	Mg2	ρ [Mpc^{-3}]
NGC 524	S0	32.5[1]	−21.40	0.356	2.390 ± 0.059	1.22 ± 0.030	3.933	0.894	0.286 ± 0.011	0.15
NGC 1023	S0	29.97[2]	−19.73	0.262	2.320 ± 0.016	1.15 ± 0.014	3.674	0.929	0.271 ± 0.002	0.57
NGC 1399	cD	31.17[8]	−21.07	0.056	2.518 ± 0.075	1.19 ± 0.003	3.428	0.937	0.330 ± 0.003	1.59
NGC 1404	E1	31.15[8]	−20.28	0.049	2.327 ± 0.096	1.21 ± 0.003	3.972	0.932	0.308 ± 0.003	1.59
NGC 3115	S0	30.2[3]	−20.44	0.205	2.424 ± 0.058	1.19 ± 0.013	3.732	0.872	0.308 ± 0.003	0.08
NGC 3379	E1	30.3[4]	−20.12	0.105	2.313 ± 0.040	1.18 ± 0.001	3.709	0.902	0.289 ± 0.002	0.52
NGC 3384	S0	30.3[4]	−19.54	0.105	2.150 ± 0.029	1.14 ± 0.022	3.721	0.895	0.277 ± 0.007	0.54
NGC 4365	E3	31.94[5]	−21.66	0.091	2.429 ± 0.021	1.24 ± 0.002	3.316	0.889	0.312 ± 0.003	2.93
NGC 4406	E	31.45[5]	−21.84	0.128	2.407 ± 0.032	1.26 ± 0.024	3.001	0.928	0.290 ± 0.003	1.41
NGC 4472	E2/S0	30.94[5]	−22.05	0.096	2.484 ± 0.037	1.18 ± 0.009	2.910	0.895	0.313 ± 0.002	3.31
NGC 4473	E5	31.07[5]	−19.98	0.123	2.280 ± 0.023	1.29 ± 0.005	3.783	0.912	0.298 ± 0.004	2.17
NGC 4486	E0/1	31.15[5]	−21.81	0.096	2.545 ± 0.029	1.28 ± 0.009	3.210	0.968	0.270 ± 0.005	4.17
NGC 4494	E1/2	30.88[6]	−20.42	0.092	2.199 ± 0.029	-	3.291	0.892	0.253 ± 0.004	1.04
NGC 4552	E0	31.00[5]	−20.47	0.177	2.422 ± 0.021	1.16 ± 0.024	3.675	0.933	0.298 ± 0.005	2.97
NGC 4594	Sa	29.8[9]	−20.61	0.221	2.385 ± 0.035	1.21 ± 0.020	3.690	0.927	0.309 ± 0.010	0.32
NGC 4649	E2	31.06[5]	−21.56	0.114	2.535 ± 0.028	1.21 ± 0.107	3.466	0.961	0.335 ± 0.003	3.49
NGC 4733	E	31.0[7]	−18.63	0.090	1.941 ± 0.054	-	3.228	0.888	0.166 ± 0.005	-

Note. — Sources for the various parameters listed in the table: Morphological types: NASA/IPAC Extragalactic Database, A_B values: Schlegel et al. (1998), $V-I$ colors and B magnitudes: Prugniel & Heraudeau (1998), Mg2 indices: Golev & Prugniel (1998), central velocity dispersions (σ_0): the Lyon/Meudon Extragalactic Database. ρ = Galaxy density in Mpc^{-3}, from Tully (1988). Distance references: [1]Radial velocity, H_0 = 75 km / sec / Mpc. [2]Ciardullo, Jacoby and Harris (1991). [3]Elson (1997). [4]Sakai et al. (1997). [5]Neilsen & Tsvetanov (2000). [6]Simard & Pritchet (1994). [7]Assumed Virgo member. [8]McMillan et al. (1993). [9]Ford et al. (1996).

Table 3: Results of the KMM test applied to data for globular clusters in the galaxies. Also listed is the probability that the color distribution is not unimodal, calculated from the "dip" statistic (P(dip)). Note P(kmm) close to 0 indicates a high probability for *bi*modality, while P(dip) close to 0 indicates a high probability for *uni*modality. Data for NGC 1399 and NGC 1404 have been converted from $B-I$ colors using the relations in Forbes & Forte (2000).

Galaxy	$(V-I)_0$	peaks	N(blue,red)		P(kmm)	P(dip)
NGC 524	0.980	1.189	360	174	0.011	0.000
NGC 1023	0.912	1.164	69	50	0.000	0.917
NGC 1399	0.952	1.185	152	256	0.000	0.999
NGC 1404	0.938	1.170	80	65	0.001	0.827
NGC 3115	0.922	1.153	53	48	0.114	0.955
NGC 3379	0.964	1.167	21	24	0.543	0.595
NGC 3384	0.942	1.207	20	9	0.009	0.000
NGC 4365	0.981	1.185	313	10	0.193	0.033
NGC 4406	0.986	1.145	117	33	0.744	0.022
NGC 4472	0.943	1.207	277	255	0.000	0.999
NGC 4473	0.936	1.157	72	48	0.098	0.375
NGC 4486	0.951	1.196	334	375	0.000	0.999
NGC 4494	0.901	1.101	65	68	0.005	0.786
NGC 4552	0.953	1.172	83	53	0.004	0.271
NGC 4594	0.939	1.184	41	56	0.007	0.363
NGC 4649	0.954	1.206	176	169	0.000	0.999
NGC 4733	0.918	1.083	18	9	0.189	0.878

Table 4. Two-parameter t_5 function fits to the globular cluster luminosity functions.

Galaxy	Range	Blue			Red			All		
		$m_V^{\rm TO}$	σ_t	N	$m_V^{\rm TO}$	σ_t	N	$m_V^{\rm TO}$	σ_t	$\Delta m_V^{\rm TO}$
NGC 524	$20.0 < V < 26.0$	$24.34^{+0.09}_{-0.15}$	$1.04^{+0.13}_{-0.10}$	320	$24.68^{+0.13}_{-0.15}$	$1.04^{+0.13}_{-0.10}$	297	$24.51^{+0.06}_{-0.12}$	$1.04^{+0.08}_{-0.07}$	$0.34^{+0.20}_{-0.18}$
NGC 1023	$19.0 < V < 24.0$	$22.82^{+0.47}_{-0.48}$	$1.80^{+0.14}_{-0.34}$	86	$23.92^{+0.32}_{-0.46}$	$1.42^{+0.27}_{-0.18}$	87	$23.53^{+0.24}_{-0.38}$	$1.62^{+0.19}_{-0.19}$	$1.10^{+0.58}_{-0.66}$
NGC 3115	$19.0 < V < 24.0$	$22.45^{+0.26}_{-0.28}$	$1.48^{+0.29}_{-0.20}$	64	$22.66^{+0.34}_{-0.32}$	$1.49^{+0.28}_{-0.21}$	51	$22.55^{+0.20}_{-0.22}$	$1.49^{+0.24}_{-0.16}$	$0.22^{+0.44}_{-0.41}$
NGC 3379	$20.0 < V < 24.0$	$22.57^{+0.30}_{-0.29}$	$1.01^{+0.56}_{-0.15}$	24	$23.02^{+0.35}_{-0.29}$	$1.09^{+0.43}_{-0.17}$	31	$22.78^{+0.22}_{-0.21}$	$1.05^{+0.32}_{-0.13}$	$0.45^{+0.45}_{-0.42}$
NGC 3384	$20.0 < V < 24.0$	$22.98^{+0.10}_{-0.13}$	$0.53^{+0.21}_{-0.02}$	30	$24.37^{+0.00}_{-0.59}$	$0.89^{+0.27}_{-0.14}$	24	$23.30^{+0.12}_{-0.13}$	$0.63^{+0.12}_{-0.07}$	$1.39^{+0.13}_{-0.60}$
NGC 4365	$20.0 < V < 25.0$	$24.01^{+0.13}_{-0.15}$	$1.12^{+0.13}_{-0.10}$	293	$24.83^{+0.09}_{-0.37}$	$1.27^{+0.15}_{-0.14}$	207	$24.37^{+0.15}_{-0.16}$	$1.22^{+0.10}_{-0.09}$	$0.81^{+0.17}_{-0.39}$
NGC 4406	$20.0 < V < 25.0$	$23.28^{+0.12}_{-0.16}$	$1.04^{+0.17}_{-0.12}$	97	$23.52^{+0.16}_{-0.18}$	$1.09^{+0.20}_{-0.13}$	77	$23.38^{+0.08}_{-0.14}$	$1.05^{+0.11}_{-0.09}$	$0.24^{+0.23}_{-0.22}$
NGC 4472	$20.0 < V < 25.0$	$23.38^{+0.14}_{-0.17}$	$1.09^{+0.20}_{-0.12}$	302	$24.21^{+0.24}_{-0.22}$	$1.42^{+0.17}_{-0.13}$	391	$23.78^{+0.12}_{-0.15}$	$1.29^{+0.12}_{-0.11}$	$0.83^{+0.29}_{-0.26}$
NGC 4473	$20.0 < V < 25.0$	$23.46^{+0.14}_{-0.16}$	$0.90^{+0.19}_{-0.10}$	68	$23.86^{+0.18}_{-0.22}$	$1.09^{+0.24}_{-0.14}$	65	$23.66^{+0.10}_{-0.14}$	$1.00^{+0.12}_{-0.11}$	$0.40^{+0.24}_{-0.26}$
NGC 4486	$20.0 < V < 25.0$	$23.36^{+0.08}_{-0.12}$	$1.25^{+0.09}_{-0.09}$	304	$23.58^{+0.06}_{-0.08}$	$1.21^{+0.05}_{-0.08}$	474	$23.50^{+0.04}_{-0.08}$	$1.22^{+0.04}_{-0.06}$	$0.22^{+0.13}_{-0.11}$
NGC 4494	$20.0 < V < 24.5$	$23.24^{+0.11}_{-0.15}$	$0.71^{+0.21}_{-0.08}$	94	$23.76^{+0.23}_{-0.20}$	$0.72^{+0.23}_{-0.07}$	68	$23.40^{+0.09}_{-0.13}$	$0.70^{+0.13}_{-0.07}$	$0.52^{+0.27}_{-0.22}$
NGC 4552	$20.0 < V < 24.5$	$23.01^{+0.20}_{-0.22}$	$1.34^{+0.33}_{-0.17}$	84	$23.61^{+0.26}_{-0.22}$	$1.22^{+0.24}_{-0.15}$	69	$23.32^{+0.14}_{-0.19}$	$1.33^{+0.19}_{-0.12}$	$0.60^{+0.34}_{-0.30}$
NGC 4594	$19.0 < V < 23.5$	$21.80^{+0.18}_{-0.20}$	$0.96^{+0.37}_{-0.11}$	41	$22.22^{+0.11}_{-0.13}$	$0.80^{+0.14}_{-0.11}$	70	$22.09^{+0.09}_{-0.11}$	$0.89^{+0.12}_{-0.09}$	$0.42^{+0.23}_{-0.22}$
NGC 4649	$20.0 < V < 25.0$	$23.46^{+0.12}_{-0.14}$	$1.33^{+0.15}_{-0.11}$	200	$23.66^{+0.10}_{-0.12}$	$1.22^{+0.11}_{-0.10}$	222	$23.58^{+0.06}_{-0.10}$	$1.28^{+0.08}_{-0.09}$	$0.20^{+0.17}_{-0.17}$
NGC 4733	$20.0 < V < 25.0$	-	-	21	-	-	18	-	-	-

Note. — The fits were carried out within the magnitude limits indicated in Fig. 2 for the 15 galaxies with V, I photometry. Both the turn-over magnitude ($m_V^{\rm TO}$) and dispersion (σ_t) of the t_5 function were allowed to vary. For NGC 4486 (M87), only the central (deep) pointing has been used. No meaningful fit could be obtained for NGC 4733. All magnitudes are corrected for Galactic foreground extinction.

Table 5. One-parameter t_5 function fits to the globular cluster luminosity functions.

Galaxy	Range	Blue		Red		All	
		$m_V^{\rm TO}$	N	$m_V^{\rm TO}$	N	$m_V^{\rm TO}$	$\Delta m_V^{\rm TO}$
NGC 524	$20.0 < V < 26.0$	$24.36^{+0.12}_{-0.14}$	320	$24.72^{+0.13}_{-0.15}$	297	$24.56^{+0.07}_{-0.13}$	$0.36^{+0.19}_{-0.20}$
NGC 1023	$19.0 < V < 24.0$	$22.45^{+0.25}_{-0.26}$	86	$23.37^{+0.40}_{-0.27}$	87	$22.93^{+0.20}_{-0.19}$	$0.92^{+0.48}_{-0.37}$
NGC 3115	$19.0 < V < 24.0$	$22.27^{+0.18}_{-0.20}$	64	$22.43^{+0.22}_{-0.22}$	51	$22.34^{+0.11}_{-0.16}$	$0.16^{+0.30}_{-0.28}$
NGC 3379	$20.0 < V < 24.0$	$22.62^{+0.35}_{-0.32}$	24	$23.03^{+0.35}_{-0.28}$	31	$22.82^{+0.21}_{-0.24}$	$0.41^{+0.47}_{-0.45}$
NGC 3384	$20.0 < V < 24.0$	$23.37^{+0.38}_{-0.29}$	30	$24.48^{+0.00}_{-0.60}$	24	$23.90^{+0.33}_{-0.27}$	$1.11^{+0.29}_{-0.71}$
NGC 4365	$20.0 < V < 25.0$	$23.98^{+0.15}_{-0.17}$	293	$24.54^{+0.28}_{-0.22}$	207	$24.22^{+0.13}_{-0.14}$	$0.56^{+0.33}_{-0.27}$
NGC 4406	$20.0 < V < 25.0$	$23.30^{+0.12}_{-0.18}$	97	$23.52^{+0.16}_{-0.18}$	77	$23.40^{+0.08}_{-0.14}$	$0.22^{+0.24}_{-0.22}$
NGC 4472	$20.0 < V < 25.0$	$23.39^{+0.13}_{-0.17}$	302	$23.89^{+0.16}_{-0.17}$	391	$23.65^{+0.09}_{-0.12}$	$0.50^{+0.24}_{-0.21}$
NGC 4473	$20.0 < V < 25.0$	$23.56^{+0.16}_{-0.20}$	68	$23.86^{+0.20}_{-0.20}$	65	$23.72^{+0.12}_{-0.16}$	$0.30^{+0.28}_{-0.26}$
NGC 4486	$20.0 < V < 25.0$	$23.30^{+0.06}_{-0.12}$	304	$23.52^{+0.06}_{-0.08}$	474	$23.44^{+0.04}_{-0.08}$	$0.22^{+0.13}_{-0.10}$
NGC 4494	$20.0 < V < 24.5$	$23.41^{+0.26}_{-0.23}$	94	$24.15^{+0.14}_{-0.47}$	68	$23.63^{+0.21}_{-0.21}$	$0.74^{+0.27}_{-0.54}$
NGC 4552	$20.0 < V < 24.5$	$22.91^{+0.15}_{-0.18}$	84	$23.52^{+0.22}_{-0.20}$	69	$23.19^{+0.11}_{-0.15}$	$0.61^{+0.28}_{-0.25}$
NGC 4594	$19.0 < V < 23.5$	$21.85^{+0.22}_{-0.24}$	41	$22.38^{+0.19}_{-0.18}$	70	$22.20^{+0.13}_{-0.15}$	$0.53^{+0.31}_{-0.28}$
NGC 4649	$20.0 < V < 25.0$	$23.34^{+0.10}_{-0.12}$	200	$23.60^{+0.08}_{-0.12}$	222	$23.48^{+0.06}_{-0.10}$	$0.26^{+0.14}_{-0.16}$
NGC 4733	$20.0 < V < 25.0$	-	21	-	18	-	-
Milky Way	$M_V < -5$	$-7.63^{+0.15}_{-0.17}$	67	$-7.17^{+0.30}_{-0.35}$	20	$-7.55^{+0.13}_{-0.15}$	$0.46^{+0.34}_{-0.38}$

Note. — The fits were carried out within the magnitude limits indicated in Fig. 2 for the 15 galaxies with V, I photometry. Only the turn-over magnitude ($m_V^{\rm TO}$) of the t_5 function was allowed to vary. For comparison we have also included fits to Milky Way globular clusters brighter than $M_V = -5$, roughly corresponding to the magnitude limit for the ellipticals. Note: the turn-over magnitudes for the Milky Way data are absolute.

Table 6: Comparison of power-law fits to the upper end of the LFs. The fits are for $10^5 L_\odot < L < 10^6 L_\odot$. Also given is a weighted mean of the power-law slopes for data with errors on the slope less than 0.5.

Galaxy	Power-law index		
	Blue	Red	All
NGC 524	-1.60 ± 0.12	-1.91 ± 0.13	-1.74 ± 0.09
NGC 1023	-1.70 ± 0.26	-2.49 ± 0.37	-2.02 ± 0.21
NGC 3115	-1.60 ± 0.31	-1.17 ± 0.34	-1.41 ± 0.22
NGC 3379	-0.80 ± 0.68	-1.23 ± 0.60	-1.00 ± 0.45
NGC 3384	-2.52 ± 0.97	-1.00 ± 1.10	-2.34 ± 0.67
NGC 4365	-1.69 ± 0.11	-1.79 ± 0.16	-1.73 ± 0.09
NGC 4406	-1.49 ± 0.19	-1.52 ± 0.23	-1.52 ± 0.15
NGC 4472	-1.66 ± 0.15	-1.87 ± 0.14	-1.78 ± 0.10
NGC 4473	-1.76 ± 0.31	-2.25 ± 0.32	-2.11 ± 0.22
NGC 4486	-1.65 ± 0.11	-1.79 ± 0.10	-1.74 ± 0.08
NGC 4494	-2.00 ± 0.23	-2.31 ± 0.37	-2.20 ± 0.20
NGC 4552	-1.43 ± 0.21	-1.56 ± 0.29	-1.61 ± 0.17
NGC 4594	-2.00 ± 0.30	-1.94 ± 0.29	-1.98 ± 0.21
NGC 4649	-1.59 ± 0.15	-1.68 ± 0.16	-1.64 ± 0.11
NGC 4733	-1.68 ± 0.71	-1.03 ± 0.49	-1.61 ± 0.37
Mean	-1.66 ± 0.03	-1.80 ± 0.06	-1.74 ± 0.04
Milky Way	-2.20 ± 0.28	-1.62 ± 0.37	-2.20 ± 0.13

Table 7: Cluster sizes for clusters brighter than $V = 24$. For the Milky Way the division between 'Blue' and 'Red' clusters is at [Fe/H] = -1. R_e= Median effective radius in pc, N = number of clusters in each bin.

					$(V-I)_0$ color range							
	Blue		Red		$[0.70-0.90]$		$[0.90-1.05]$		$[1.05-1.20]$		$[1.20-1.45]$	
Galaxy	R_e	N	R_e	N	R_e	N	R_e	N	R_e	N	R_e	N
NGC 524	2.76	135	2.59	92	2.99	27	2.76	108	2.76	70	2.07	22
NGC 1023	1.72	84	1.65	71	1.65	36	1.79	48	1.22	49	3.73	22
NGC 1399	1.99	113	1.37	212	2.12	33	1.99	80	1.37	122	1.37	90
NGC 1404	1.61	43	1.61	47	1.98	12	1.36	31	1.61	30	1.48	17
NGC 3115	2.47	70	2.23	56	2.71	26	2.39	47	2.31	44	2.23	16
NGC 3379	3.01	26	2.25	31	3.53	6	2.93	20	2.09	19	2.76	12
NGC 3384	2.34	28	3.34	15	2.34	13	2.34	15	3.34	6	5.34	9
NGC 4365	2.40	163	2.88	79	2.76	56	2.31	107	2.84	66	3.44	13
NGC 4406	4.11	78	2.98	57	4.82	20	3.83	58	3.26	40	2.84	17
NGC 4472	1.85	220	1.46	249	1.79	59	1.91	161	1.57	120	1.23	129
NGC 4473	2.02	61	1.90	44	2.41	26	1.79	35	1.90	37	2.38	8
NGC 4486	2.59	580	2.04	757	3.09	179	2.47	401	2.16	437	1.85	320
NGC 4494	2.07	97	1.82	61	2.26	35	1.96	62	1.82	55	3.38	6
NGC 4552	1.96	87	1.97	80	2.42	26	1.96	61	1.73	50	2.07	30
NGC 4594	1.81	56	1.43	84	2.27	16	1.81	40	1.62	42	1.17	42
NGC 4649	1.66	157	1.30	175	2.01	34	1.66	123	1.30	88	1.42	87
NGC 4733	2.88	16	1.40	7	3.00	6	2.88	10	1.40	7	0.0	0
Milky Way	3.24	96	2.29	39	3.28	60	3.03	36	2.37	24	2.07	15

Table 8: Cluster sizes and $V-I$ colors for blue and red clusters (brighter than $V = 24$) for different radial bins in selected cluster-rich galaxies.

Galaxy	R_e(med,pc)		N(blue)	N(red)	$(V-I)_0$	
r in arcmin	Blue	Red			Blue	Red
NGC 4472						
$0.0 < r < 0.5$	2.27	1.66	18	25	0.96	1.20
$0.5 < r < 1.0$	1.91	1.23	45	46	0.97	1.19
$1.0 < r < 1.5$	1.91	1.40	40	63	0.94	1.20
$1.5 < r < 2.0$	1.68	1.57	38	43	0.95	1.24
$2.0 < r < 3.0$	1.85	1.23	43	46	0.93	1.22
$3.0 < r < 4.0$	1.79	1.96	36	26	0.94	1.19
NGC 4486						
$0.0 < r < 0.5$	2.84	2.00	70	168	0.95	1.19
$0.5 < r < 1.0$	2.35	1.85	150	242	0.96	1.19
$1.0 < r < 1.5$	2.66	2.16	169	190	0.93	1.18
$1.5 < r < 2.0$	2.84	1.98	83	81	0.94	1.19
$2.0 < r < 3.0$	2.66	2.53	81	64	0.93	1.14
$3.0 < r < 4.0$	2.41	2.10	47	22	0.93	1.22
$4.0 < r < 6.0$	2.35	2.59	40	22	0.94	1.17
$6.0 < r < 9.0$	2.59	2.84	35	14	0.92	1.20
NGC 4365						
$0.0 < r < 0.5$	3.56	2.88	34	13	0.95	1.16
$0.5 < r < 1.0$	1.78	2.84	44	18	0.92	1.04
$1.0 < r < 1.5$	1.78	1.95	44	20	0.91	1.10
$1.5 < r < 2.5$	3.91	3.20	21	13	1.01	1.32
$2.5 < r < 3.5$	5.15	5.51	17	13	0.92	1.14

Table 9: Sizes for metal-poor and metal-rich GCs in the Milky Way in three radial bins.

	R_e(med,pc)		N([Fe/H] < -1)	N([Fe/H] > -1)
	[Fe/H] < -1	[Fe/H] > -1		
$R_g < 2$ kpc	2.33	1.98	13	14
$2 < R_g < 5$ kpc	2.56	2.38	19	15
$5 < R_g < 10$ kpc	3.03	2.52	20	7

Table 10: Slopes, Spearman correlation coefficients (ρ) and the probability that correlations are present (P_C) for various host galaxy parameter vs. GC color relations.

	Blue GCs			Red GCs		
	Slope	ρ	P_C	Slope	ρ	P_C
M_B	-0.016 ± 0.005	-0.64	98.9%	-0.020 ± 0.008	-0.45	92.6%
$\log \sigma_0$	0.075 ± 0.035	0.51	95.8%	0.156 ± 0.042	0.53	96.5%
$(V-I)_0$	0.176 ± 0.120	0.39	85.6%	-0.098 ± 0.120	0.03	9.6%
Mg2	0.262 ± 0.147	0.38	86.8%	0.667 ± 0.158	0.43	91.6%
$(B-K)_0$	-0.007 ± 0.020	-0.12	37.6%	0.017 ± 0.028	-0.00	1.2%
$(J-K)_0$	0.158 ± 0.226	0.24	66.1%	0.480 ± 0.306	0.34	82.3%